A PATH INTEGRAL MONTE CARLO METHOD FOR THE QUASIELASTIC RESPONSE

Thesis by

Carlo Carraro

In Partial Fulfillment of the Requirements

for the Degree of

Doctor of Philosophy

California Institute of Technology

Pasadena, California

1990

(Submitted May 21, 1990)

Acknowledgments

I would like to thank Steve Koonin for his guidance through this and other projects, for introducing me to computational physics, and for continuous material and intellectual support.

I am indebted to several people for helpful and stimulating conversations, in particular to Michael Cross and Ryoichi Seki. I would like to thank my office mates, as well as all the other "Kellogites" who have contributed to make work at the Laboratory enjoyable.

During my stay at Caltech, I have been supported by the friendship of many special people, particularly Roya, Andreas, Francisco, Mike, Shouleh, and Wolfgang.

On a more prosaic side, this work was supported in part by the National Science Foundation.

Abstract

We formulate the quasielastic response of a non-relativistic many-body system at zero temperature in terms of ground state density matrix elements and real time path integrals that embody the final state interactions. While the former provide the weight for a conventional Monte Carlo calculation, the latter require a more sophisticated treatment. We argue that the recently developed Stationary Phase Monte Carlo technique can be used to study the approach to "Y-scaling." We perform calculations for a particle in a potential well in one and three dimensions and compare them to the exact results available for these models. We then derive an eikonal approximation to the Path Integrals. This method is suitably generalized to treat strongly repulsive interactions, and allows comparison to Silver's theory of final state interactions in a straightforward way. We also give an exact prescription to calculate the scaling limit for potentials comprising a hard core. Finally, we study the approach to scaling in a model ^{4}He nucleus, and find good agreement with experimental data.

Table of Contents

List of Figures

Chapter 1
Introduction

Inelastic scattering is a very useful experimental tool in many-body physics. This is because, in Born approximation, the inelastic cross section is proportional to the dynamic structure factor (or dynamic response) of the many-body system, $S(\vec{q},\omega)$. Different probes (e.g., electrons, neutrons, x-rays) can be used to study a variety of systems, from solids to liquids, from atoms to nucleons. A suitable choice of energy and momentum transfers $(\omega,\vec{q})$ allows the experimenter to focus on one of several different aspects of the many-body system, such as collective modes or single particle properties.

This thesis deals with quasielastic (QE) scattering, which involves energy and momentum transfers much higher than the characteristic scale of the collective modes. QE scattering can be viewed as a two-body collision between the probe and one of the constituents of the many-body system. Many-body effects come into play because the initial momentum of the struck constituent is determined by a probability $n(k)$ (the one-body momentum distribution) and because the struck particle can interact with the other particles during its recoil (final state interaction).

At high momentum transfers, if the recoil kinetic energy can be assumed to be much larger than the interparticle potential, final state interactions (FSI) are expected to become negligible, thus making QE scattering an effective means of probing the single particle momentum distribution of the many-body system. This assumption is called the impulse approximation (IA) and leads to the phenomenon of Y-scaling

[1], [2]; i.e., the fact that $qS(\vec{q},\omega)$ depends solely upon the "scaling" variable $Y \equiv M\omega/q - q/2$, M being the mass of the struck particle, and not separately upon q and ω (we assume non-relativistic kinematics unless otherwise specified). Remarkably, in the IA, the momentum distribution $n(k)$ can be extracted from the QE cross section in a completely model-independent fashion. This fact is of obvious interest to the theorist. Fundamental ideas such as Bose condensation [1] in liquid ^{4}He can be tested, and our ability to calculate equilibrium properties of many-body systems can be checked, together with our knowledge of the interaction potential between the constituents. For example, powerful computational techniques, such as Green function Monte Carlo [3] or path integral Monte Carlo [4] (PIMC), have been used to calculate the ground state of quantum liquids. The situation in nuclear physics is less satisfactory, as the short range behavior of the internucleon force is still not understood completely.

What do we learn from the experimental data available for both quantum liquids and atomic nuclei? Unfortunately, connection between data and theory is less straightforward than the naive IA suggests. Indeed, interatomic forces (and nuclear forces to a lesser extent) are characterized by a short range, highly repulsive component—almost a hard core—which undermines the picture of free particle recoil [5]. Consider a particle initially sitting in the long range, weakly attractive potential well due to its neighbors. After being struck by the probe, it will recoil with high momentum (i.e., essentially free) until it bounces from the "hard wall" presented by one of its neighbors' short range repulsive potential. This will happen even at high recoil momenta. Furthermore, in real experiments, only a finite range of momentum transfers is available, and it may well be that even the long range attractive part of the potential has to be taken into account in trying to unravel the effects of the FSI.

This problem is particularly severe in nuclear physics. Here QE scattering is limited to the region of negative Y, where the energy transfer is low enough that inelastic processes (such as Δ-resonance excitation) are unimportant. Therefore, the nucleon recoil energy is at best about 10 times its binding energy. For comparison, momentum transfers as high as 24 Å^{-1} have been achieved in QE scattering from liquid ^{4}He [6], yielding typical recoil energies about 100 times the binding energy. One can observe some differences between the response at such high momentum transfers and that at lower ones (e.g., $q = 7$ Å^{-1}), corresponding to those available in nuclear physics experiments.

There is an important difference between QE scattering experiments in quantum liquids and in atomic nuclei. High backgrounds prevent neutron scattering experiments from measuring small cross sections. Therefore the QE response of liquid He is measured accurately only for small $|Y|$ (i.e., over less than two orders of magnitude in intensity). Fortunately, this is the domain of interest in the search for the Bose condensate. The QE response of nuclei, instead, is subject to more substantial errors at small $|Y|$, arising from inelastic processes, whereas at larger $|Y|$ (and $Y < 0$) it can be measured accurately over several orders of magnitude.

Clearly, it would be desirable to develop a first-principles calculation of the dynamic response given a realistic potential to provide a link between the observed quasielastic cross sections and the inferred momentum distributions. In view of the success of stochastic methods in calculating many-body equilibrium properties, such as ground state wave functions and static correlation functions, it is natural to ask whether analogous methods can be applied to the calculation of a dynamic property such as the QE response. An important ingredient in the success of these static calculations is a well-chosen trial function embodying much of the physics. Fortunately,

for the QE response, the IA can provide an analogous zeroth order approximation to guide the calculation.

Although there are no conceptual obstacles toward this end, there is an as yet insurmounted practical difficulty when one tries to develop a stochastic method to perform quantum dynamics calculations. The evaluation of a static property can be reduced to averaging an observable over a sampling weight function in a rather straightforward way, at least for Bose systems. For instance, matrix elements of the imaginary time evolution operator provide such a weight in the PIMC method. Quantum dynamics, on the other hand, requires that the evolution operator matrix elements be evaluated in real time, or that the imaginary time matrix elements be analytically continued onto the real axis. In the latter case, [7] the problem is essentially equivalent to inverting a Laplace transform, an extremely ill-posed numerical problem. In the former case, real-time evolution turns Boltzmann-like factors into oscillatory exponentials, for which stochastic sampling methods have long looked hopeless. Recently, however, Doll, Freeman and co-workers [8] have devised a new technique, the stationary phase Monte Carlo (SPMC) method, to evaluate oscillatory integrals by sampling the integrand more densely near the points of constructive interference.

Although SPMC is still far from being a general purpose quantum dynamics technique, it is a good candidate for a first-principles non-relativistic calculation of the QE response, formulated in terms of path integrals. This is suggested by the following argument. The problems introduced by the evaluation of path integrals in real time become obviously less and less severe the shorter the timescale involved, as long as the potential remains finite. An estimate of the important time scale in QE scattering is given by the ratio of the characteristic lengthscale of the problem, set by

the equilibrium density matrix, to the velocity of the recoiling particle, determined by the momentum transfer $\vec{q}$. Thus only short times are important at high momentum transfers and one legitimately expects the SPMC method to give a satisfactory answer. This very argument led Gersch *et al.* [9] to develop a $1/q$ expansion for the FSI.

Following this reasoning, we first develop a formulation of the QE response in which the IA is multiplicatively corrected by a real time path integral between two ground state configurations of the many-body system. We propose to evaluate the path integral, which embodies the FSI, by the SPMC method. Second, we test the principle of this method by applying it to a one-body system in an external potential well. This problem is exactly soluble in 1D and easily treated numerically in 3D. Next we turn to strong potentials, such as the ones encountered in real systems, which require a special treatment. Finally, we solve a more realistic problem and calculate the QE response of a ^{4}He nucleus, using a state-independent, central potential, that has been already employed successfully for static calculations by other authors [10].

This thesis is organized as follows. In Ch. 2, we set up the QE response formalism, introduce the concept of "Y-scaling", illustrate it (together with its own limitations) with experimental results from condensed matter and nuclear systems, and briefly review the relevant theoretical background. In Ch. 3, we derive the path integral formulation of the response, which allows us to establish Y-scaling and scaling violations. In Ch. 4, we review the SPMC technique and develop it in a way that is best suited to our problem. In Ch. 5, we present our numerical methods and results for the one-body problem, (both MC and exact calculations), and we also compare the SPMC method to the stationary phase method when possible. In Ch. 6, we address the problem of strong potentials and hard cores. Finally, in Ch. 7, we present the calculation for ^{4}He and compare it to experiment.

Chapter 2
Quasielastic Response and "Y Scaling"

2.1 The Inclusive Cross Section and the Impulse Approximation

Consider a system of N particles (the target) interacting via a many-body potential (which we assume to be spin and isospin independent for simplicity) and an external probe, interacting weakly with the constituents of the system. We are interested in the rate of the inclusive process in which the probe scatters from the target transferring momentum $\vec{q}$ and energy ω, and the final state of the target is not resolved experimentally.

Let $|\psi_i\rangle$ and $|\psi_f\rangle$ be the initial and final states of the N-body system; the transition matrix element between these states is given, in Born approximation, by

$$\begin{aligned} T_{if} &= \int d^3x_1 \cdots d^3x_N d^3x dt \psi_f^*(\vec{x}_1 \ldots \vec{x}_N, t) e^{-i(\vec{k}-\vec{q})\cdot\vec{x}+i(E_f-\omega)t} \\ &\qquad \sum_j v(\vec{x}-\vec{x}_j) e^{i(k\cdot\vec{x}-E_i t)} \psi_i(\vec{x}_1 \ldots \vec{x}_N, t) \qquad (2.1) \\ &= \hat{v}(-\vec{q}) \langle \psi_f | \hat{\rho}(-\vec{q}) | \psi_i \rangle \delta(E_f - E_i - \omega)\,, \end{aligned}$$

where the density operator $\hat{\rho}(q)$ is simply the Fourier transform of the one-body density of the system (e.g., the charge density for Coulomb scattering). By Fermi's golden rule, we obtain the transition rate between initial and final state

$$\sigma_{if}(\vec{q},\omega) = 2\pi \left|\hat{v}(-q)\right|^2 \left|\langle \psi_f | \hat{\rho}(-\vec{q}) | \psi_i \rangle\right|^2 \delta(E_f - E_i - \omega). \qquad (2.2)$$

Because the final state of the target is undetermined, the rate of the inclusive process is calculated by summing over all possible $|\psi_f\rangle$. This yields

$$\sigma(\vec{q},\omega) = 2\pi \left|v(q)\right|^2 NS(\vec{q},\omega), \tag{2.3}$$

which defines the dynamic response, or structure factor,

$$S(\vec{q},\omega) \equiv \sum_f |\langle\psi_f|\hat{\rho}(-\vec{q})|\psi_i\rangle|^2 \delta(E_f - E_i - \omega). \tag{2.4}$$

This definition is convenient because it separates the physics of the target (i.e., the many-body system) from that of the probe and from the kinematics. An integral representation of the energy δ-function allows us to rewrite the structure factor explicitly as the Fourier transform of the time-dependent density-density correlation function:

$$S(\vec{q},\omega) = \frac{1}{2\pi N} \int dt\, e^{i\omega t} \langle \rho_{-\vec{q}}(t) \rho_{\vec{q}}(0) \rangle \,, \tag{2.5}$$

where $\langle\ \rangle$ indicates the ground state average or, at finite temperature, the average over the thermal density matrix describing the state of the target, and the Heisenberg operators $\rho_{\vec{q}}(0)$ and $\rho_{-\vec{q}}(t)$ respectively inject momentum $\vec{q}$ into the system at time 0 and remove it at time t:

$$\rho_{\vec{q}}(t) = \sum_{i=1}^{N} e^{i\vec{q}\cdot\vec{r}_i(t)}. \tag{2.6}$$

The expression we have just derived can be extended easily to relativistic form (appropriate for high energy electron-nucleus scattering). We simply replace the density operator $\rho(\vec{x},t)$ by the 4-current $j^\mu(x)$, to get the explicitly covariant response tensor

$$W^{\mu\nu}(p) = \frac{1}{2\pi N} \int d^4x\, e^{ip\cdot x} \langle j^\mu(x) j^\nu(0) \rangle.$$

It is easy to recognize that W^{00} reduces to $S(\vec{q},\omega)$ in the non-relativistic limit. In what follows, we will remain within the workframe of non-relativistic quantum mechanics, unless otherwise specified.

It is convenient to split the response into two parts, according to whether the particle absorbing momentum $\vec{q}$ is or is not the same one to give it up after time t. We thus define the incoherent response

$$S^i(\vec{q},\omega) = \frac{1}{2\pi N}\int dt\, e^{i\omega t}\langle \sum_i e^{-i\vec{q}\cdot\vec{r}_i(t)} e^{i\vec{q}\cdot\vec{r}_i(0)}\rangle\,, \tag{2.7}$$

and the coherent response

$$S^c(\vec{q},\omega) = \frac{1}{2\pi N}\int dt\, e^{i\omega t}\langle \sum_{i\neq j} e^{-i\vec{q}\cdot\vec{r}_i(t)} e^{i\vec{q}\cdot\vec{r}_j(0)}\rangle\,. \tag{2.8}$$

In the IA, as we discussed in the previous chapter, FSI are neglected. Thus the struck particle recoils freely,

$$r_i(t) = r_i(0) + (q + k_i)t/m,$$

and one can write

$$e^{-i\vec{q}\cdot\vec{r}_i(t)} e^{i\vec{q}\cdot\vec{r}_i(0)} |\vec{k}_1,\ldots,\vec{k}_N\rangle = e^{-i(\vec{q}\cdot\vec{k}_i + q^2/2)t} |\vec{k}_1,\ldots,\vec{k}_N\rangle.$$

Insertion of complete momentum eigenstates into Eq. 2.7 leads to

$$S^i(\vec{q},\omega) = \frac{1}{2\pi}\int dt d^3k\, n(\vec{k}) e^{i\omega t} e^{-i(\vec{q}\cdot\vec{k}_i + q^2/2)t}, \tag{2.9}$$

whereupon the incoherent response scales to a function of the single variable

$$Y \equiv \omega/q - q/2 \tag{2.10}$$

(we set the mass of the constituents equal to one for the moment):

$$S^i_{IA}(\vec{q},\omega) = \frac{1}{4\pi^2 q}\int_{|Y|}^{\infty} dk\, k\, n(k)\,, \tag{2.11}$$

where $n(k)$ is the one-body momentum distribution. Therefore, in the IA, the QE cross section can be calculated from the static properties of the ground state or thermal ensemble of the many-body system. A similar treatment of S^c leads to an expression that falls off very rapidly with q compared to S^i. This happens because the coherent response probes the ground state density matrix at momenta of order q (typically much larger than Y). An explicit expression for S^c_{IA} will be derived in the next chapter.

Experimentally, one defines the functions

$$F^{i(c)}(q,Y) \equiv qS^{i(c)}(\vec{q},\omega) \tag{2.12}$$

and looks for scaling by considering the behavior of qS at fixed Y as q increases. In the IA, one expects F^c to vanish at high q, while F^i approaches the q-independent function

$$F^i_{IA}(Y) = \frac{1}{4\pi^2}\int_{|Y|}^{\infty} dp\, p\, n(p)\,, \tag{2.13}$$

from which the momentum distribution can be obtained simply by differentiating with respect to Y:

$$n(k) = -\frac{4\pi^2}{k}\frac{d}{dY}F^i_{IA}(Y)\Big|_{Y=k}. \tag{2.14}$$

2.2 Review of experimental results

Quasielastic scattering at high momentum transfers provides a way of measuring the momentum distribution through the "scaling" relation Eq. 2.14; this has been known for well over 20 years, [1] although the introduction of the term "Y-scaling" is more recent [2]. The method was first applied to condensed matter systems.

Perhaps the most interesting application is the measurement of the momentum distribution of liquid ^{4}He (LHe). ^{4}He atoms obey Bose statistics and LHe is experimentally found to have a superfluid transition at $T_\lambda = 2.17$ K at standard pressure. Below T_λ, the behavior of LHe reveals the presence of a macroscopic quantum state, and it is natural to ask whether this can be identified with the Bose condensate. By measuring the momentum distribution above and below T_λ one should be able to detect macroscopic occupancy of the zero-momentum state, if Bose condensation occurs [1]. Indeed, substituting into Eq. 2.13

$$n(k) = n_0 \delta_{k,0} + n'(k),$$

where $n'(k)$ is the excited states momentum distribution (i.e., that of the normal state of LHe), one finds

$$F(Y) = n_0 \delta(Y) + \frac{1}{4\pi^2} \int_{|Y|}^{\infty} dk\, k\, n'(k)\,, \tag{2.15}$$

that is, $F(Y)$ now shows a δ-function peak at $Y = 0$. Obviously, this peak will be broadened by experimental resolution and also by FSI, and its detection by comparison with the normal state $F(Y)$ is highly non-trivial. Indeed even for temperatures

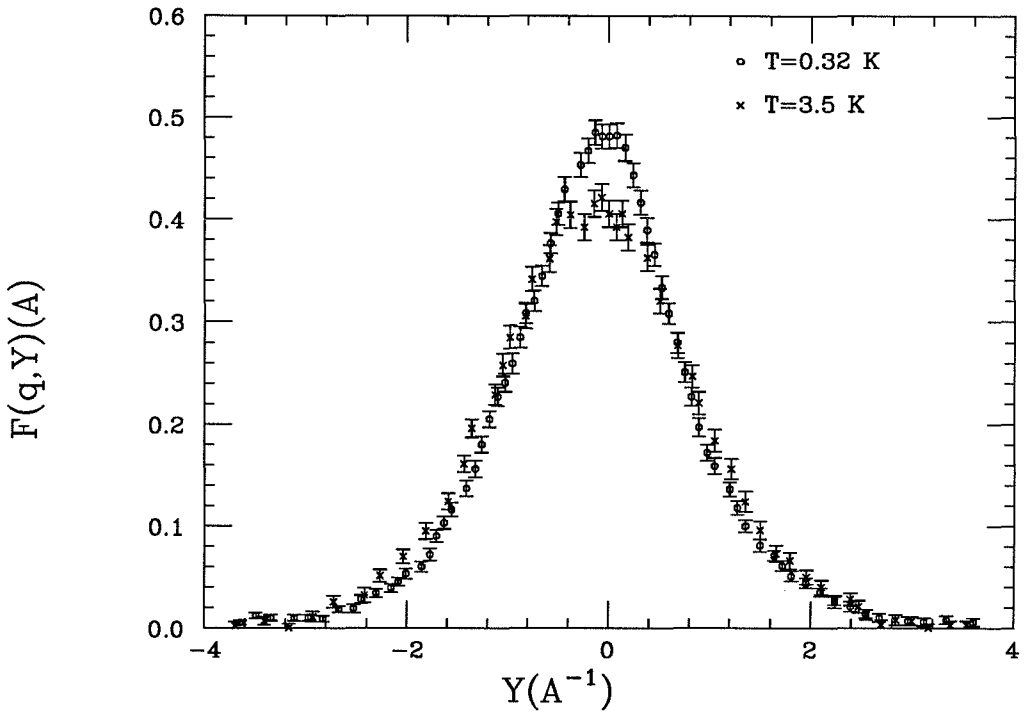

Figure 2.1 – Dynamic response of liquid ^{4}He near the quasielastic peak, at momentum transfer $q = 24$ Å^{-1} and temperatures $T = 3.5$ and 0.32 K. The excess strength around $Y = 0$ for the $T = 0.32$ K data is attributed to a $\sim$ 10% Bose condensate peak, broadened by experimental resolution and final state interactions.

as low as a few tenths of a Kelvin, where the superfluid fraction approaches 100%, the condensate fraction certainly doesn't exceed ~10% [11].

Fig. 2.1 shows a comparison of measurements of $F(Y)$ at 3.5 and 0.32 K [11]. These measurements are carried out by inelastic neutron scattering. Momentum transfers as large as 24 Å^{-1} have been used. Because one finds appreciable differences between the $q = 7$ and the $q = 24$ data [11], it would be important to reach even higher momentum transfers.

QE scattering has been widely used in nuclear physics experiments as well. Here "Y-scaling" is expected only for negative Y; for $Y \gtrsim 0$, the energy transferred to the

nucleon is high enough to excite its internal degrees of freedom, so that the picture of a point-like nucleon breaks down. This point is well illustrated in Fig. 2.2, showing the QE response of ^{12}C measured by electron scattering. Thus the interest is focussed on large negative Y. Probing $n(k)$ at large momenta is a way of testing nuclear interactions at short distances (this is impossible to achieve by nucleon-nucleon scattering at high energy, again because of inelastic effects).

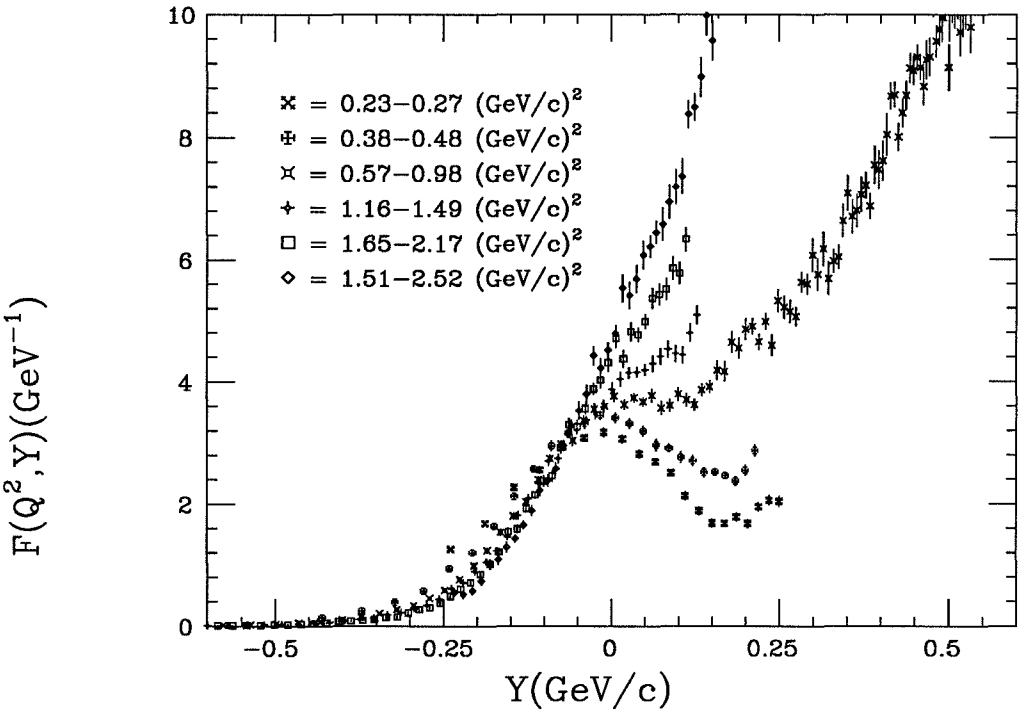

Figure 2.2 – Longitudinal response of ^{12}C, from electron scattering data. Inelastic processes are dominant for $Y \geq 0$. The Q^2 range is shown for each curve.

Fig. 2.3 shows the QE response of ^{4}He, ^{12}C, ^{56}Fe, and ^{197}Au, as measured by the NE3 collaboration at SLAC [12] [13].

One can see that the data display quite impressive scaling behavior over several orders of magnitude in $F(Y)$. However, a closer look at the data, at fixed Y, reveals

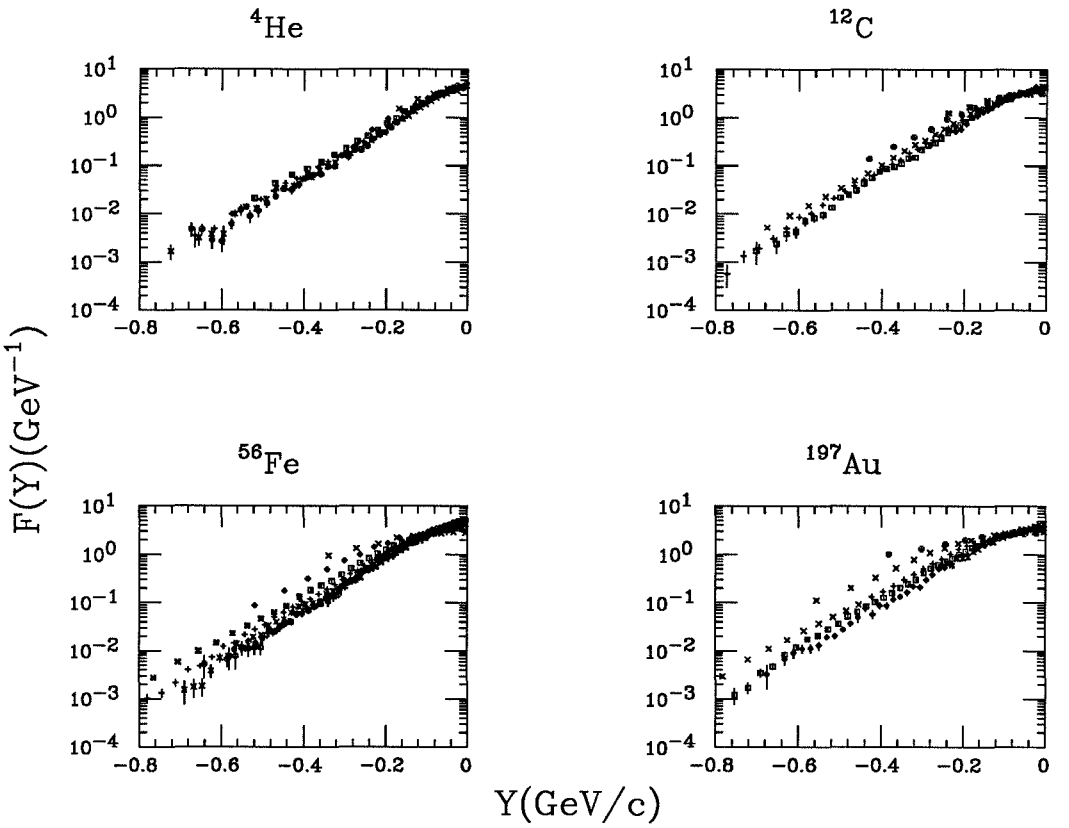

Figure 2.3 – Quasielastic electron scattering from nuclei for several different kinematics. The response is extracted from the measured cross sections as described in Ref. [13]. Scaling behavior is displayed over several orders of magnitude, but strong scaling violations are also visible. Note the logarithmic vertical scale.

that the response does indeed show a residual q-dependence, that can be as large as 100% (Fig. 2.4). This observation [14] raises the question of the importance of FSI in nuclear physics.

2.3 Review of theories of FSI

Several calculations of FSI have been performed for both neutron scattering from quantum liquids and electron scattering from nuclei. The first appeared in the work of Hohenberg and Platzmann[2] [1] on QE neutron scattering and the IA for liquid ^{4}He, and was based on the following simple considerations. The response at high q is dominated by the pole at the single-particle recoil energy, $E_r = \omega + Y^2/2M$. The

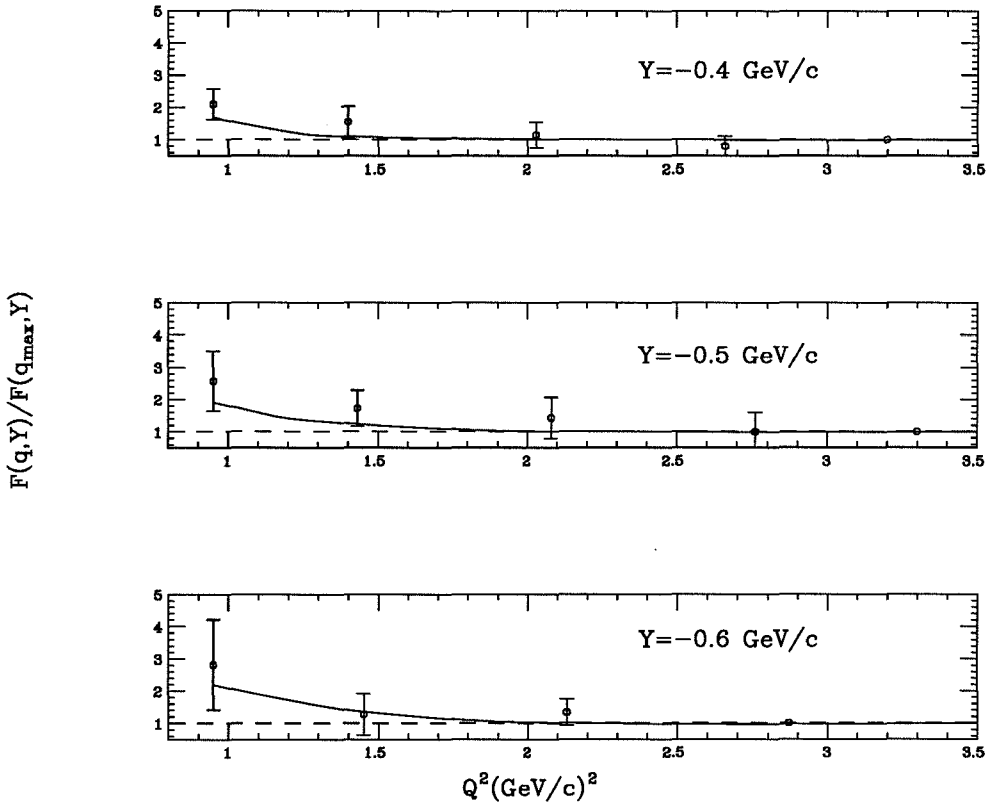

Figure 2.4 – The quasielastic response of ^{56}Fe at fixed Y for increasing momentum transfer suggests that scaling may not have been attained at the actual experimental kinematics (scaling behavior requires that $F(Q^2, Y)$ be independent of Q^2 at fixed Y). Here, Q^2 is minus the four-momentum transfer.

effect of collisions during the recoil results in a mean free path, or lifetime, of the recoiling particle, which gives the energy E_r an imaginary part. This shows up as a broadening of the QE peak. In this ansatz, the effect of FSI can be accounted for by convolving the IA structure factor with a lorentzian broadening function:

$$\begin{aligned} F(Y) &= \int_{-\infty}^{\infty} dY' R(Y - Y') F_{IA}(Y') \\ R(Y) &= \frac{1}{\pi} \frac{\Gamma}{Y^2 + \Gamma^2} = \mathrm{Re} \frac{1}{\pi} \int_0^{\infty} dx e^{iYx - \Gamma x} \end{aligned} \tag{2.16}$$

where the width Γ is related to the mean free path λ as follows:

$$\Gamma = \frac{1}{2\lambda} = N\sigma(q)/2V.$$

Thus, $R(Y)$ is simply the Fourier transform of the probability that there be no collision as the particle recoils between 0 and x. For hard spheres of radius a, $\sigma = 2\pi a^2$, whereby

$$\Gamma = \frac{N}{V}\pi a^2 . \tag{2.17}$$

For a strongly repulsive potential, one can choose an effective, momentum transfer-dependent hard core radius a such that

$$\sigma(q) \simeq 2\pi a^2.$$

More relevant to the work developed in this thesis is the calculation by Gersch *et al.* [9] who were able to expand the structure factor as a sum of integrals of many-body correlation functions, the expansion parameter being the inverse of the momentum transfer q. At $q \to \infty$, the response is given by the lowest order term, which they found to be exactly the IA. In this way, they could calculate not only the broadening of the QE peak in neutron scattering from LHe, but also its shift toward lower Y due to FSI at finite q. However, these results are only qualitatively correct; the extracted value of the condensate fraction is about 3%, lower than more refined calculations suggest ($n_0 \sim 9\%$).

In fact, the theory is not applicable to strong two-body interactions. The reason can be understood qualitatively for hard core (HC) interactions, where the scattering amplitude, which can be regarded as a renormalized potential, grows linearly with q. Therefore, $O(V/q)$ corrections to the IA cannot be expected to vanish at high q. Indeed, as shown by Weinstein and Negele [5] with a perturbative calculation of the HC Bose gas, although Y-scaling is still observed asymptotically, the scaling function is not related in an obvious way to the momentum distribution.

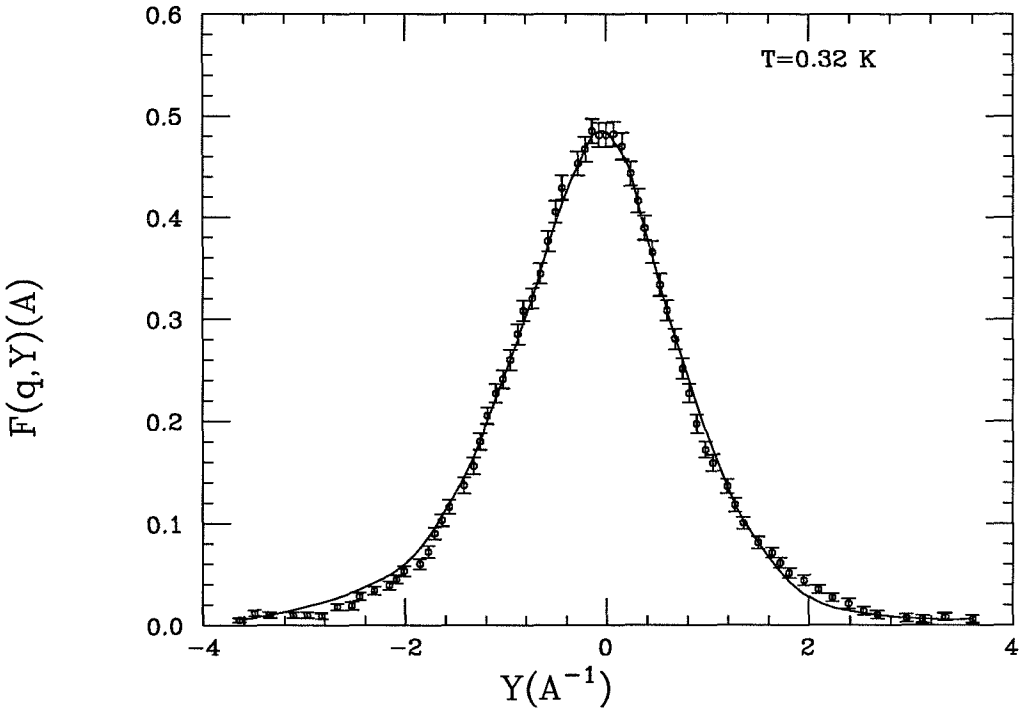

Figure 2.5 – Hard Core Perturbation Theory fit to the dynamic response of superfluid liquid ^{4}He near the quasielastic peak (q = 24 Å^{-1}; T =0.32 K. The theory includes empirical experimental resolution and final state interactions.

The persistence of correlation effects in the infinite-q limit is also a feature of Silver's theory of FSI, named "Hard Core Perturbation Theory" [15]. Like Hohenberg and Platzman, he predicts a convolution form for the QE response, but the broadening function he derives, largely from semiclassical arguments, is not a lorentzian. Despite its abstruse formulation, this theory simply amounts to replacing

$$x\Gamma \equiv x\frac{N}{V}\pi a^2$$

in Eq. 2.16 with $\int_0^x dz\Gamma(z)$, where the collision rate per unit length, $\Gamma(z)$, is taken to be

$$\Gamma(z) \equiv \frac{N}{V}2\pi \int_0^a dbbg(\sqrt{b^2+z^2}) \tag{2.18}$$

where g is the pair correlation function of the liquid. This theory is in excellent agreement with neutron scattering data from liquid ^{4}He (Fig. 2.5); it is expected to be successful at very high momentum transfers, which have been attained in neutron scattering, but its relevance to QE electron scattering is far from being clear [16].

An *exact* expression for the $q \to \infty$ limit of $F(Y)$ for a many-body system interacting through an arbitrary potential containing a hard core has been derived recently by Gurvitz, Rinat, and Rosenfelder [17] employing the concepts of geometric optics. We will derive the same expression in Sec. 6.4, using the path integral formalism that we are going to establish in the next chapter. Thus we refer to Chapter 6 for a detailed treatment of this theory.

This brief (and by no means exhaustive) review of theories of FSI indicates that they generally suffer from one or more of the following limitations: low order truncation of the perturbation expansion, inconsistent treatment of the static (ground state) and dynamic (final state) properties, unrealistic (e.g., pure hard core) potentials. Therefore, it would be desirable to develop a first-principles calculation of the dynamic response given a realistic potential to provide a link between the observed quasielastic cross sections and the inferred momentum distributions.

Chapter 3
Path Integral Representation of the QE Response

Functional integrals are probably the most elegant way of approaching the many-body problem and deriving perturbation expansions [18]. They also provide a way to get nonperturbative results, as often required in treating strongly interacting systems. In what follows, however, we shall introduce and develop functional integrals simply because they are the only tractable (nonperturbative) numerical technique for solving the many-body problem.

3.1 The Dirac-Feynman Path Integral

We start by recalling the Dirac-Feynman formulation of quantum mechanics. We work with a single particle in one dimension for simplicity. Let H be the hamiltonian operator (again, we put $m = 1$)

$$H = T + V = P^2/2 + V.$$

The Schrödinger equation

$$i\frac{\partial}{\partial t}|\psi\rangle = H|\psi\rangle \tag{3.1}$$

is formally solved by

$$|\psi(t)\rangle = e^{-iHt}|\psi(0)\rangle. \tag{3.2}$$

The time evolution operator e^{-iHt} is called the propagator, because the knowledge of its matrix elements allows one to "propagate" the wavefunction in space-time:

$$\psi(x',t) = \int dx K(x',x;t)\psi(x,0), \tag{3.3}$$

where

$$K(x',x;t) \equiv \langle x'|e^{-iHt}|x\rangle. \tag{3.4}$$

Therefore, knowing the propagator is equivalent to having solved the Schrödinger equation (its Green's function is indeed $G = -iK$). For the free particle, the solution is found easily by inserting a resolution of unity in terms of momentum eigenstates:

$$\langle x'|e^{-iH_0t}|x\rangle = \int \frac{dp}{2\pi}\langle x'|p\rangle\langle p|e^{-itp^2/2}|x\rangle = \frac{1}{\sqrt{2\pi it}}e^{i(x\prime-x)^2/2t}. \tag{3.5}$$

If $V \neq 0$, a problem arises from the non-commutativity of V and T:

$$\exp(it(T+V)) = \exp(itT)\exp(itV)\exp(-t/2[V,T]+\cdots)$$
$$[V,T] = (V'' + 2iV'P)/2.$$

Thus, if the operator $[V,T]$ is finite (as is the case if the potential is well-behaved), the error made by neglecting the commutator goes to zero, as the time interval $\epsilon \to 0$, as ϵ^2:

$$\exp(i\epsilon(P^2/2+V)) = \exp(i\epsilon P^2/2)\exp(-i\epsilon V) + O(\epsilon^2)$$

Upon inserting a complete set of momentum eigenstates, one has

$$\begin{aligned} K(x',x;\epsilon) &= e^{-i\epsilon V(x)}\int \frac{dp}{2\pi}e^{ip(x\prime-x)}e^{-i\epsilon p^2/2} + O(\epsilon^2) \\ &= \frac{1}{\sqrt{2\pi i\epsilon}}e^{i(x\prime-x)^2/2\epsilon - i\epsilon V(x)} + O(\epsilon^2),\ \epsilon \to 0. \end{aligned} \tag{3.6}$$

This suggests how to proceed for finite t. By slicing up the time, $\epsilon \equiv t/N$, and inserting complete sets of position eigenstates in the definition above at each timeslice, we derive a most useful convolution identity:

$$\begin{aligned} K(x',x;t) &= \langle x'|(e^{-iH\epsilon})^N|x\rangle \\ &= \int dx_1 \ldots dx_{N-1} K(x',x_{N-1};\epsilon)K(x_{N-1},x_{N-2};\epsilon)\ldots K(x_1,x;\epsilon). \end{aligned} \tag{3.7}$$

Note that the sequence of positions at subsequent time intervals

$$\{x_j\} = (x_0 \equiv x, x_1, \ldots, x_{N-1}, x_N \equiv x')$$

defines a continuous, albeit not differentiable, path in coordinate space; hence the term "Path Integral."

By convolving the short time propagator with itself $N-1$ times, we get

$$K(x',x;t) = \frac{1}{\sqrt{2\pi i\epsilon}} \int \prod_{j=1}^{N-1} \frac{dx_j}{\sqrt{2\pi i\epsilon}} e^{i\sum_{j=1}^{N} \frac{(x_j - x_{j-1})^2}{2\epsilon} - i\epsilon \sum_{j=1}^{N} V(x_j)}, \tag{3.8}$$

where have neglected a remainder that goes to zero as $N \to \infty$ (or equivalently $\epsilon \to 0$). The remainder can be made higher order in ϵ by rearranging the kinetic and potential energy terms in the hamiltonian; for instance, writing $H = V/2 + T + V/2$ yields

$$K(x',x;\epsilon) = \frac{1}{\sqrt{2\pi i\epsilon}} e^{i(x\prime - x)^2/2\epsilon - i\epsilon(V(x)+V(x\prime))/2} + O(\epsilon^3), \quad \epsilon \to 0, \tag{3.9}$$

while the expression for $K(x',x;t)$ is changed only at the endpoints of the path.

It is interesting to observe that the argument of the exponential is nothing but the discrete approximation of the action along the path $\{x_j\}$; indeed, as $\epsilon \to 0$, we have

$$\{x_j\} \to x(\tau)$$
$$\sum_{j=1}^{N} \frac{(x_j - x_{j-1})^2}{2\epsilon} - \epsilon \sum_{j=1}^{N} V(x_j) \to \int_0^t d\tau \Big(\frac{1}{2} \Big(\frac{dx}{d\tau} \Big)^2 - V(x(\tau)) \Big), \tag{3.10}$$

and it is conventional to use the shorthand notation

$$K(x', x; t) = \int_x^{x'} \mathcal{D}[x(\tau)] e^{iS(x,t)}. \tag{3.11}$$

Path integrals are particularly appealing because they are a rigorous approach to quantum mechanics, but at the same time allow us to exploit our intuition for classical systems (the concept of path is purely classical). We shall see how this proves useful below. It is worthwhile to mention that functional integrals can be applied with equal success to statistical mechanics. The replacement $it \equiv \beta$ in the discussion above yields a path integral representation of the Boltzmann factor $\exp(-\beta H)$ (where now the paths are defined in imaginary time, or inverse temperature); this, combined with stochastic integration techniques, provides one of the most powerful tools in modern theoretical physics.

We conclude this brief introduction by observing that Eq. 3.11 is trivially extended to arbitrary number of particles N in a space of arbitrary dimension d. All one has to do is to write down the action for the many-body system, and consider all the possible paths in a $d \times N$ configuration space.

3.2 The response operator

In this section, we apply the path integral formalism to the calculation of the (scaled) QE response

$$qS(q,\omega) = \frac{q}{2\pi N}\int dt e^{i\omega t} < e^{iHt}\rho_{-\vec{q}}e^{-iHt}\rho_{\vec{q}} > . \tag{3.12}$$

We recall that we have set $\hbar = 1$ and, in the rest of this chapter, we can also put $m = 1$ without loss of generality. We start by inserting complete sets of position eigenstates:

$$q\,S(\vec{q},\omega) = \int dx\,dx'\varrho(x,x')\Omega(x',x) \tag{3.13}$$

Here x denotes the ensemble of all the particle coordinates; these are $n = N \times d$ in number for N particles in d dimensions. $\varrho(x,x')$ is the density matrix element and

$$\Omega(x',x) = q\int \frac{dt}{2\pi N}\, e^{i\omega t}\sum_{i,j}\int dx_0 \langle x'|e^{iHt}|x_0\rangle\langle x_0|e^{-iHt}|x\rangle\, e^{i\vec{q}\cdot(\vec{x}_i-\vec{x}_j^{\,0})} \tag{3.14}$$

is the "response operator." We now introduce path integral representations of the propagators forward and backward in time

$$\begin{aligned}
\langle x_0|e^{-iHt}|x\rangle &= \int_x^{x_0}\mathcal{D}[x_+(\tau)]\exp\Big(i\int_0^t d\tau\Big(\tfrac{1}{2}\Big(\frac{dx_+}{d\tau}\Big)^2 - V(x_+)\Big)\Big) \\
\langle x'|e^{iHt}|x_0\rangle &= \int_{x_0}^{x'}\mathcal{D}[x_-(\tau)]\exp\Big(-i\int_0^t d\tau\Big(\tfrac{1}{2}\Big(\frac{dx_-}{d\tau}\Big)^2 - V(x_-)\Big)\Big) .
\end{aligned} \tag{3.15}$$

Consider the incoherent response first. For a finite interaction potential V, we expect that the main contribution to S^i comes from the IA, Eq. (2.13); in fact, this is a rigorous result [19]. As discussed in the previous section, this corresponds to considering a free-particle recoil. Therefore, a good starting point will be to shift to

new path integration variables $z_\pm(\tau)$ centered around the path of the freely recoiling particle:

$$\begin{aligned} x_+(\tau) &= z_+(\tau) + (x_0 - x)\frac{\tau}{t} + x \\ x_-(\tau) &= z_-(\tau) + (x_0 - x')\frac{\tau}{t} + x' \end{aligned} \tag{3.16}$$

(so that $z_\pm(0) = z_\pm(t) = 0$) and to substitute $x_0 \to x_0 + (x + x')/2$, thus obtaining

$$\begin{aligned} \Omega^i(x', x) = q \int \frac{dt}{2\pi}\, e^{i\omega t} \int \frac{dx_0}{(2\pi|t|)^n} \exp\Big(-iqx_{0\|} + iq\frac{(x-x')_\|}{2} - ix_0\frac{(x-x')}{t}\Big) \\ \times \int_0^0 \mathcal{D}z_+\mathcal{D}z_- \exp\Big(i\int_0^t d\tau(\tfrac{1}{2}(\frac{dz_+}{d\tau})^2 - V_+)\Big) \exp\Big(-i\int_0^t d\tau(\tfrac{1}{2}(\frac{dz_-}{d\tau})^2 - V_-)\Big). \end{aligned} \tag{3.17}$$

The subscript $\|$ denotes the coordinate of the recoiling particle along the momentum transfer vector $\vec{q}$; we will use the subscript $\perp$ to indicate all the remaining $n-1$ coordinates (the "spectators"). $V_\pm$ is the potential evaluated along the paths $x_\pm(\tau)$. The first line of the formula above depicts a particle receiving momentum $\vec{q}$ at time zero, propagating in a straight line between x and x_0 forward in time t, and then backward to x' after giving up momentum $\vec{q}$. The path integrals in the second line describe the quantum fluctuations around this classical picture, as well as the interactions within the many-body system. The IA and the approach to scaling, however, are not yet evident. A few more algebraic steps are needed, which again are suggested by the physics.

As we argued at the end of the previous section, we expect shorter and shorter time scales to be relevant to QE scattering as the momentum transfer grows larger and larger. In such a short time, the struck particle will propagate a finite distance along the direction of its high-speed recoil (i.e., parallel to $\vec{q}$), while the motion in the other directions (and that of the other particles in the system) will tend to be frozen. (Incidentally, we note that this picture is not justified in presence of

strong interactions, when "billiard ball" collisions can take place. However, when we deal with hard cores in Ch. 6, we shall see that we can still employ these ideas, in the eikonal approximation.) As we are dealing here with finite interactions, we choose new sets of coordinates in line with our reasoning. We introduce velocities by defining $x_0 \equiv vt$ and explicitly scale time by the inverse of the momentum transfer, $t \equiv (\xi - 1)(x - x')_{\|}/q$. Notice that now particles moving at finite velocity will travel only distances $\sim 1/q$. The recoil velocity, $v_{\|}$, has to be proportional to q, so we set $v_{\|} \equiv (\kappa + 1)\omega/q$. Upon introducing these changes of variables, we arrive at

$$\Omega^i(x', x) = \frac{1}{2\pi} e^{-iY(x-x')_{\|}} \int \frac{d\kappa\, d\xi}{2\pi}\, e^{-i\kappa\xi} \times \int \frac{d^{n-1}v_{\perp}}{(2\pi)^{n-1}}\, e^{-iv(x-x')_{\perp}} \int_0^0 \mathcal{D}\zeta_+\, \mathcal{D}\zeta_-\, e^{i(S_+ - S_-)} \tag{3.18}$$

$$S_{\pm} = \frac{1}{2}\int_0^1 d\sigma \left(\frac{d\zeta_{\pm}}{d\sigma}\right)^2 - \frac{(x - x')_{\|}}{q}(\tilde{\xi} - 1)\int_0^1 d\sigma\, V_{\pm}(z_{\pm}; \tilde{\xi}, \tilde{\kappa}, v/q; x, x'; \sigma)\ , \tag{3.19}$$

where $\sigma \equiv \tau/t$ is the scaled time, $\tilde{\xi} \equiv \xi/\sqrt{\frac{\omega|x-x'|_{\|}}{q}}$, $\tilde{\kappa} \equiv \kappa/\sqrt{\frac{\omega|x-x'|_{\|}}{q}}$ and $z_{\pm} \equiv \zeta_{\pm}\sqrt{|t|}$. Notice that $\tilde{\xi}$, $\tilde{\kappa}$ and $z_{\pm}$ are all suppressed as $1/\sqrt{q}$ at high q; i.e., at high momentum transfers, the argument of the potential becomes independent of the fluctuations around the free-particle recoil. We emphasize that Eqs. 3.18, 3.19, although derived largely from intuitive arguments, is formally exact.

Before we discuss the result we have just derived, we rewrite Eq. 3.19 using a Fourier representation of the path, which makes the kinetic energy diagonal (i.e., local) in the path coordinates. This will prove convenient in the next sections, as well as for computational purposes. Because the endpoints of the paths are fixed ($\zeta_{\pm}(\sigma = 0) = \zeta_{\pm}(\sigma = 1) = 0$), we can write

$$\zeta_{\pm}(\sigma) = \frac{\sqrt{2}}{\pi}\sum_{m=1}^{\infty}\frac{1}{m}\eta_{m\pm}\sin(m\pi\sigma), \tag{3.20}$$

so that the action becomes

$$S_{\pm} = \sum_{m=1}^{\infty} \eta_{m\pm}^2/2 - \frac{(x-x')_{\|}}{q}(\tilde{\xi}-1)\int_0^1 d\sigma\, V_{\pm}. \tag{3.21}$$

The argument of the potential will be written down explicitly in a later chapter.

Equation 3.18 reveals that we have succeeded in separating the IA contribution from terms that are of order $1/q$ or higher. Indeed, since we are considering finite two-body interactions, if we let $q \to \infty$, we easily recover the IA, Eq. 2.13, as all integrals in Eq. 3.18 become trivial, yielding

$$\Omega_{IA}^{i}(x',x) = \frac{1}{2\pi} e^{-iY(x-x')_{\|}} \delta^{(n-1)}(x-x')_{\perp}\,. \tag{3.22}$$

It has long been known that the $O(1/q)$ correction to the IA can be written down in a rather straightforward fashion. This is also easily derived from Eq. 3.18. We simply expand

$$\exp\Big(-i\frac{(x-x')_{\|}}{q}(\tilde{\xi}-1)\int_0^1 d\sigma\, V_{\pm}\Big) \simeq 1 + i\frac{(x-x')_{\|}}{q}\int_0^1 d\sigma\, V_{\pm} \tag{3.23}$$

and evaluate the potential at the zeroth order path in $1/q$ ($z_{\pm}=0$), to obtain

$$\begin{aligned}\Omega_1^i(x',x) =& \frac{i}{2\pi q} e^{-iY(x-x')_{\|}} \delta^{(n-1)}(x-x')_{\perp}\,(x-x')_{\|} \\ &\times \int_0^1 d\sigma\,(V(x-(x-x')_{\|}\sigma) - V(x')).\end{aligned} \tag{3.24}$$

Upon substituting Eq. 3.24 into Eq. 3.13, we recover Eq. 31 of Ref. [9].

We turn now to the coherent response. We rewrite the matrix elements of the density operator in Eq. 3.14 as follows

$$e^{i\vec{q}\cdot(\vec{x}_i-\vec{x}_j^0)} = e^{i\vec{q}\cdot(\vec{x}_j-\vec{x}_j^0)} e^{i\vec{q}\cdot(\vec{x}_i-\vec{x}_j)}.$$

Therefore, grouping the identical contributions from all pairs, we obtain

$$q\,S^c(\vec{q},\omega) = (N-1)\int dx\,dx'\varrho(x,x')e^{i\vec{q}\cdot(\vec{x}_1-\vec{x}_2)}\,\Omega^i(x',x); \tag{3.25}$$

i.e., our discussion of the matrix elements $\Omega^i(x',x)$ remains unchanged, the only difference being a "coherence" factor multiplying the density matrix. This factor is responsible for the rapid decay of the coherent response at high q, where it measures the probability of finding two particles with very high momenta in the equilibrium density matrix of the system.

Now that we have set up the path integral formalism in a way that makes the approach to scaling quite transparent, we are left with the problem of carrying out the integrations. These are of two different kinds: Eq. 3.13 is the average of the response operator $\Omega(x',x)$ weighed by the density matrix elements $\varrho(x,x')$; we expect standard MC techniques to be suitable for this calculation. However, Equation 3.18 is a high dimensional oscillatory integral, which we propose to evaluate by the SPMC method.

Chapter 4
The Stationary Phase Monte Carlo Method

4.1 The Monte Carlo Method

In the previous chapter, we have exploited the path integral formalism to write the QE response as a multidimensional integral. This often gives one a lot of insight in the many-body problem, as we have seen. Further, it provides a practical computational tool, if the integrals can be evaluated stochastically. The reason is that the precision of the result improves as the square root of the number of evaluations, N_s, of the integrand, because of a statistical error $O(1/N_s^{1/2})$ (as expected from a method based on the central limit theorem) [20]. Instead, for conventional quadrature methods (or direct integration of the Schrödinger equation) the error is $O(1/N_s^{\gamma/D})$ in D dimensions (the actual value of γ depends on the quadrature scheme used, e.g., $\gamma = 4$ for Simpson's rule). Therefore, stochastic quadrature outperforms conventional quadrature as soon as $D > 8$. But there is also another reason, that can become compelling for small D. Often the main contributions to a physical observable come from a very small, a priori unknown, region in phase space. It is greatly advantageous, in terms of "signal to noise" ratio, that the observable be preferentially sampled over those more important regions; usually "importance sampling" can be incorporated into the Monte Carlo method in a very straightforward fashion.

The following simple example illustrates the basics of stochastic integration, or Monte Carlo method. Consider the integral

$$I = \int_V d^D x f(x). \tag{4.1}$$

Now write

$$f(x) = g(x)p(x), \tag{4.2}$$

with

$$\begin{aligned} \int_V d^D x p(x) &= 1 \\ p(x) &\geq 0\,, \end{aligned} \tag{4.3}$$

so that the original integrals becomes

$$I = \frac{\int_V d^D x g(x) p(x)}{\int_V d^D x p(x)}\,. \tag{4.4}$$

We shall hereafter use the shorthand notation

$$I = < g >_p$$

for any integral of this kind, i.e., that is expressed as the average of an observable g with weight p. Note that in many problems of interest, integrals already come in this form. For example, in statistical mechanics, the average of the physical observable O function of the coordinates $\{x\}$ is given by

$$< O >= \frac{\int_V d^D x O(x) \exp(-\beta H(x))}{\int_V d^D x \exp(-\beta H(x))}\,. \tag{4.5}$$

In any case, once the integral has been cast in the form of Eq. 4.4, one proceeds by drawing N_S independent samplings $\{x_i\}$ of the probability function $p(x)$, and approximates the integral by

$$I_{N_s} = \frac{1}{N_s} \sum_1^{N_s} g(x_i)\,. \tag{4.6}$$

One can show [20] that as N grows large, I_N becomes normally distributed around around I, with standard deviation

$$\sigma_{N_s} = (< g^2 >_p - < g >_p^2)^{1/2} / \sqrt{N_s}\,, \tag{4.7}$$

which allows one to write

$$I = I_{N_s} \pm \sigma_{N_s}\,.$$

This approximation becomes in principle exact as $N_s \to \infty$, but in practical cases, as already mentioned, an appropriate choice of the weight $p(x)$ allows one to obtain sufficiently small variances σ at finite N_s, as evident from Eq. 4.7. This is called "importance sampling." The Stationary Phase Monte Carlo method involves the construction of such weight. Numerous other examples can be found in the literature.

4.2 The Principles of the SPMC Method

In view of the problem we set out to solve, namely the evaluation of the path integrals in Eq. 3.18, it is crucial to investigate the existence of a good sampling weight for the oscillatory integrals that occur in a generic quantum dynamics problem [21]. Many of the results reported in this section were originally derived by Doll, Freeman and coworkers (DF), who were motivated by the need of calculating dynamic correlations at finite temperature [22], i.e., functions of the type

$$C_{AB}(t) = \mathrm{tr}(\exp(-\beta H)\, A\, \exp(iHt)\, B\, \exp(-iHt))/\mathrm{tr}(\exp(-\beta H)). \tag{4.8}$$

This bears a strong resemblance to our problem, which nonetheless is complicated by the fact that we work in frequency space and, above all, that we formulate the correlation function in a way (see Eqs. 3.13, 3.14) that forces us to work with integrals

of pure phase factors. Thus, while DF have studied extensively [22],[8] the model problem

$$\int dx\rho(x)\exp(if(x)) \Big/ \int dx\rho(x)\,, \tag{4.9}$$

where $\rho(x)$ is a smooth probability distribution stemming from the Boltzmann factor, we have to face integrals of the type [see Eq. 3.18]

$$\int dx\exp(if(x))\,. \tag{4.10}$$

In any case, the strategy is to follow DF's basic idea: to generate a weight for a MC calculation that samples the integrand more densely in the regions where the phase interference is constructive; i.e., near the stationary points. Let us consider the following one-dimensional example, for which generalization to arbitrary dimension is straightforward.

Starting from the identity

$$I \equiv \int dx\, e^{if(x)} = \int dx\, e^{if(x)} \int dy\, P(y)\, e^{i(f(x-y)-f(x))}, \tag{4.11}$$

where $P(y)$ is a normalized "probability" function ($\int dyp(y) = 1$), peaked around the origin, we write

$$D(x) \equiv \int dy\, P(y)\, e^{i(f(x-y)-f(x))} \simeq \int dy\, P(y)\, e^{-iyf'(x)} \equiv D_1(x), \tag{4.12}$$

whereupon

$$I = \int dx\, D_1(x)\, e^{if(x)} \Big(1 + \frac{D(x) - D_1(x)}{D_1(x)}\Big). \tag{4.13}$$

This is convenient if the r.h.s. integral in Eq. 4.12 can be done easily. This is the case if $P(y)$ is a gaussian, $P(y) = e^{-y^2/2\epsilon^2}/\sqrt{2\pi\epsilon^2}$, as we will assume hereafter. The function

$$D_1(x) = e^{-(\epsilon f'(x))^2/2} \tag{4.14}$$

is called the SPMC filter. If ϵ is small enough, $D_1(x)$ is a good approximation for $D(x)$ and one can hope to be able to evaluate the difference $\delta D(x) \equiv D(x) - D_1(x) \ll D(x)$ with a few-point MC calculation:

$$\delta D(x) = \langle D(x) - D_1(x) \rangle_{P(y)} . \tag{4.15}$$

The integral (4.13) has the pleasant feature that the function $D_1(x)$ now provides a good weight for a stochastic evaluation of I:

$$I = \mathcal{N} \Big\langle e^{if(x)} \Big(1 + \frac{\delta D(x)}{D_1(x)} \Big) \Big\rangle_{D_1(x)}, \tag{4.16}$$

where $\mathcal{N} = \int dx\, D_1(x)$ denotes the normalization of D_1 and we use the notation $\langle \cdots \rangle_{D_1}$ to denote average with the weight function D_1. This weight samples preferentially around the stationary points of the original integral (4.10) (where f' is small), helping to filter the signal from the noise. An obvious complication is that one has to normalize the sampling weight (i.e., calculate $\mathcal{N}$). This is in general exceedingly harder at zero temperature (see Eq. (4.10)) than it is at finite temperature (Eq. (4.9)), where one can cautiously seek help in the identity

$$I = \Big\langle e^{if(x)} \Big(1 + \frac{\delta D(x)}{D_1(x)} \Big) \Big\rangle_{D_1(x)\rho(x)} \Big\langle D_1(x) \Big\rangle_{\rho(x)} . \tag{4.17}$$

Fortunately, in the application of (4.16) to our problem, we need not worry about the normalization of the weight, which turns out to be straightforward, as we will see below.

Instead, a more serious problem is encountered in applying this method to evaluating a real time path integral such as that given in Eq. 3.18. Indeed, the main contribution to the phase (i.e., to the action) comes from the kinetic energy, which is a quadratic form in the integration variables. Let us consider the trivial integral $I = \int dx\, e^{ix^2/2}$ (this integral has also been considered by DF, though still in the context of "finite temperatures"). The SPMC filter is a gaussian, $e^{-\epsilon^2 x^2/2}$, decaying too slowly to filter the noise coming from the oscillations of the integrand. However, quadratic phases offer the advantage that the function $D(x)$ can be evaluated *exactly*:

$$D(x) = (1 - i\epsilon^2)^{-1/2} \exp\Big(-\frac{\epsilon^2}{1+\epsilon^4}\frac{x^2}{2}\Big)\ \exp\Big(-i\frac{\epsilon^4}{1+\epsilon^4}\frac{x^2}{2}\Big). \tag{4.18}$$

Now, since $\delta D(x) \equiv 0$, ϵ can be chosen arbitrarily and the integral becomes

$$I = \frac{1}{\sqrt{1-i\epsilon^2}} \int dx\, \exp\Big(i\frac{x^2}{2}\frac{1}{(1+\epsilon^4)}\Big)\ \exp\Big(-\frac{x^2}{2}\frac{\epsilon^2}{(1+\epsilon^4)}\Big). \tag{4.19}$$

The second exponential provides the weight for a MC calculation of the oscillatory integral. Furthermore, a good choice for ϵ ($\epsilon \geq 1$) will suppress the oscillations, as the phase has acquired a factor $1/(1+\epsilon^4)$.

If the phase in I is of the type $f(x) = (x^2/2 - V(x))$, we simply replace x in Eq. (4.18) by $x - V'(x)$, thus obtaining an approximation for $D(x)$, $D_2(x)$, that is correct up to terms $O(V'')$:

$$D_2(x) = (1 - i\epsilon^2)^{-1/2} \exp\Big(-\frac{\epsilon^2}{1+\epsilon^4}\frac{(x-V'(x))^2}{2}\Big) \exp\Big(-i\frac{\epsilon^4}{1+\epsilon^4}\frac{(x-V'(x))^2}{2}\Big)\ . \tag{4.20}$$

In this case, however, the choice of ϵ is less obvious than for a quadratic phase. One has to compromise between high values of ϵ, which dramatically improve the signal to noise ratio but make a MC calculation of $\delta D \equiv D - D_2$ impractical, and low values of ϵ, which yield the correct result but with extremely large variance. We shall be content with choosing $\epsilon \sim 1$ and ignoring δD [23] (we observe that $\delta D \sim O(V'')$ and thus expect it to be reasonably small, when working with finite, smooth potentials; this issue will be addressed more rigorously in the next section).

In this way, we can write

$$I \simeq I_2 = \int dx w(x) \Big(\frac{D_2(x)}{w(x)} \Big) \exp(if(x)) \Big/ \int dx w(x) \,, \tag{4.21}$$

and the only problem left is the choice of the normalized weight $w(x)$ to be used in the MC evaluation of I_2. For this, we propose to take the normalized probability distribution

$$w(x) = \exp\Big(-\frac{\epsilon^2}{1+\epsilon^4} \frac{x^2}{2} \Big) \Big/ \sqrt{2\pi \frac{(1+\epsilon^4)}{\epsilon^2}} . \tag{4.22}$$

Once again, we expect this choice to be appropriate whenever the phase is largely a quadratic function of the coordinates.

4.3 Simple Examples

The SPMC approach to quantum dynamics is still in its infancy. The literature offers not more than a handful of essentially trivial examples where the method has been applied successfully [8] [22] [23] [24] [25] [26]. This makes it hard to appreciate its potential and limitations thoroughly. In the following, we try to build up our intuition by solving some simple one-dimensional integrals (not directly related to any physical problem).

Consider the integral representation of the Airy function

$$\mathrm{Ai}(t) = \frac{1}{2\pi} \int dx e^{i(tx - x^3/3)}. \tag{4.23}$$

Using the notation of the previous section, $\rho(x) = 1$ for all x and the SPMC weight is

$$D_1(x) = \exp(-\epsilon^2 (x^2 - t)^2 / 2). \tag{4.24}$$

Hereafter, we take $t = 1$.

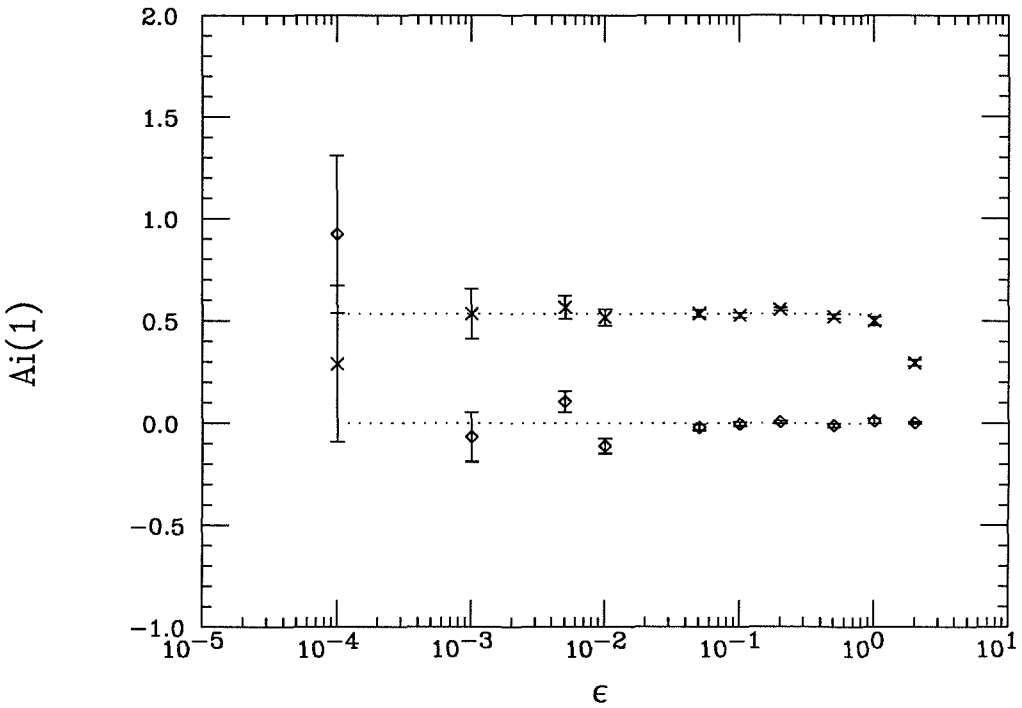

Figure 4.1 – Real (×) and imaginary part of the Airy function integral representation (Eq. 4.23), obtained by the SPMC method with $N_s = 4000$ and $N_y = 10$. The dotted lines represent the exact value.

The normalization $\mathcal{N}$ of this weight is calculated easily by a standard integration routine available in the IMSL library. The calculation of the Airy function thus requires only two MC averages (see Eq. 4.17), one weighted by $D_1(x)$ for the observable, and one weighted by a gaussian for the correction $\delta D(x)$ (Eq. 4.15). The latter has to be carried out for each one of the N_s samplings of the observable, and it is therefore desirable to perform a small number of samplings $N_y \ll N_s$.

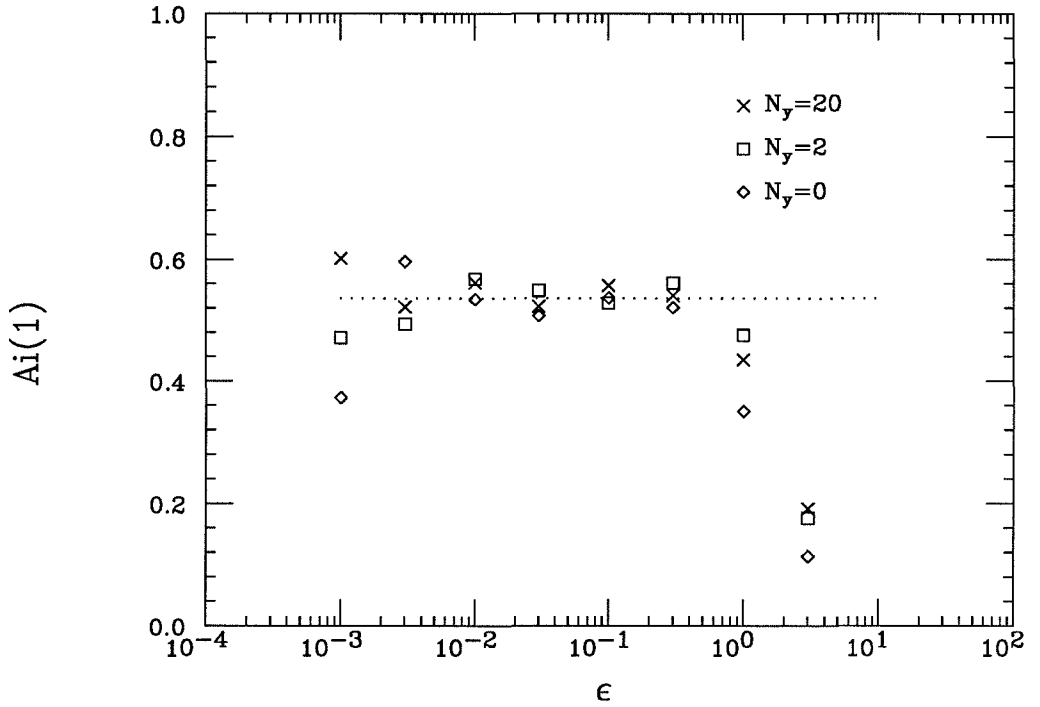

Figure 4.2 – Real part of the Airy function integral representation, obtained by SPMC. The different curves show the effect of increasing the number of points used in sampling the correction δD. The error bars for each values of ϵ are comparable to those displayed in Fig. 4.1.

In Fig. 4.1, we plot the results for Ai(1) obtained with $N_s = 4000$, $N_y = 10$, as a function of ϵ. It is quite clear that the noise becomes considerably smaller as we increase ϵ; however a systematic error shows up for $\epsilon \geq 2$. One would think

that slightly increasing N_y eliminates this inconvenient; but this is not the case even for N_y as high as a few hundred, where the computation is already extremely time-consuming (of course one eventually has to recover the right answer as $N_y \to \infty$). The dependence of the result on N_y is shown in Fig. 4.2. From this example, it appears that for $\epsilon \sim 0.1$, where δD can be safely ignored, or readily computed with a few-point calculation, the SPMC method offers a thirty-fold improvement over the brute-force ($\epsilon = 0$) evaluation of the oscillatory integral.

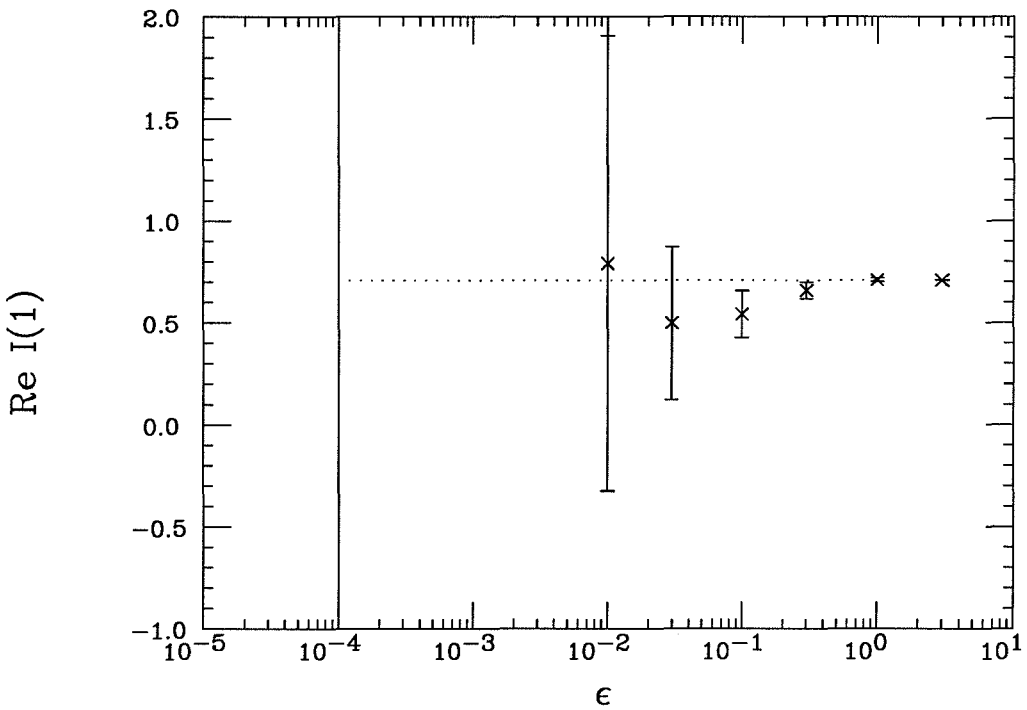

Figure 4.3 – The oscillatory gaussian integral (Eq. 4.25) with SPMC; $N_s = 4000$.

Let us consider now the integral

$$I(t) = \frac{1}{\sqrt{2\pi}} \int dx e^{-itx^2/2}. \tag{4.25}$$

Now the statistical errors are considerably larger, and the choice of ϵ would normally be much less obvious than before. In this case, it is advantageous to follow the method outlined at the end of the previous section, which allows one to evaluate integrals of quadratic phases with large ϵ and no systematic error. The effect of doing so is illustrated in Fig. 4.3.

4.4 Validity and Limitations of the SPMC Method

Given that in some interesting applications (e.g., QE scattering, as treated in this thesis) the SPMC filter can only be evaluated approximately, it is important to assess the validity of such approximations. In particular, we want to discuss the validity of our approximation for nearly quadratic phases. To do so, we start from the exact path integral for the response operator (Eq. 3.18)

$$\Omega^i(x',x) = \frac{1}{2\pi} e^{-iY(x-x')_\parallel} \int \frac{d\kappa\, d\xi}{2\pi}\, e^{-i\kappa\xi} \times \int \frac{d^{n-1}v_\perp}{(2\pi)^{n-1}}\, e^{-iv(x-x')_\perp} \int_0^0 \mathcal{D}\zeta_+\, \mathcal{D}\zeta_-\, e^{i(S_+ - S_-)} \tag{4.26}$$

$$S_\pm = \frac{1}{2}\int_0^1 d\sigma \left(\frac{d\zeta_\pm}{d\sigma}\right)^2 - \frac{(x-x')_\parallel}{q}(\tilde{\xi}-1)\int_0^1 d\sigma\, V_\pm(z_\pm;\tilde{\xi},\tilde{\kappa};x,x';\sigma) \tag{4.27}$$

Here we assume that the $v_\perp$ integration, whose main contribution to the phase is linear, can be done reliably (we shall take on this point in the next chapter). In the remaining integrals, the phase is predominantly a quadratic function of η (the sine-transform of ζ, according to Eq. 3.20), κ, and ξ. We want to show that, if the κ, ξ integrals can be handled in a controlled way, the approximation (4.20) is essentially equivalent to a loop expansion. This is not surprising, because our method accounts exactly for the kinetic energy, and approximates the potential energy, neglecting some terms of order V'' or higher.

Consider the path integral

$$\int_0^0 \mathcal{D}\zeta_+ \, \mathcal{D}\zeta_- \, e^{i(S_+ - S_-)} \, . \tag{4.28}$$

Upon slicing up the time (and using a Fourier representation of the path), this becomes the iteration of a prototype integral

$$\int \frac{dx}{\sqrt{2\pi i t/N}} e^{ix^2/2(t/N) - iV(x)t/N} \, . \tag{4.29}$$

We rewrite this trivially as

$$\int \frac{dx}{\sqrt{2\pi i}} e^{ix^2/2 - iV(x\sqrt{t/N})t/N} \tag{4.30}$$

(taking $t > 0$ for concreteness). The exact SPMC filter is given by the integral

$$\begin{aligned} D(x) &= \int \frac{dy}{\sqrt{2\pi\epsilon_x}} e^{-y^2/2\epsilon_x^2} e^{iy^2/2 - iyx} e^{-i\left(V(\sqrt{t/N}(x-y)) - V(\sqrt{t/N}x)\right)t/N} \\ &= \int \frac{dy}{\sqrt{2\pi\epsilon_x}} e^{-y^2/2\epsilon_x^2(1-i\epsilon_x^2)} e^{-iy\left(x - (t/N)^{3/2} V\prime(\sqrt{t/N}x)\right)} e^{-iy^2(t/N)^2 V\prime\prime(\sqrt{t/N}x)/2 + \ldots} \, . \end{aligned} \tag{4.31}$$

If the potential is finite and smooth, to be definite, of order one (this can always be if units are chosen appropriately), then the error we make by approximating $D(x)$ with Eq. 4.20 is found to be of order

$$y^2(t/N)^2 \sim \epsilon_x^2 (t/N)^2 \, ; \tag{4.32}$$

here we recall (Sec. 3.2) that

$$t = (1 - \xi)(x - x')/q \, , \tag{4.33}$$

where $(x-x')$ is the typical lengthscale of the density matrix. Now, the ξ, κ integrals are in turn carried out by SPMC; in these integrations, the parameter ϵ can (and should) be chosen independent of ϵ_x. Let us call it ϵ_l. Then ξ turns out to be of order ϵ_l. Thus we find

$$t \sim \epsilon_l \frac{(x-x')}{q}\,, \tag{4.34}$$

so that we want this condition to be fulfilled:

$$\epsilon_x^2(\epsilon_l(x-x')/qN)^2 \ll 1\,. \tag{4.35}$$

We shall typically use $\epsilon_l \lesssim 1$, so that we demand

$$\epsilon_x(x-x')/qN \ll 1\,. \tag{4.36}$$

Evidently, the higher N we choose, the better our approximation for the SPMC weight will be. However, since N determines the dimension of the oscillatory integral, it won't be convenient to choose it too large, because in that case we would need a very high value of ϵ_x to reduce the noise. Again, we emphasize that one has to look for an optimal intermediate range of N, ϵ_x.

Finally, it is important to point out that the method we have presented is similar to the stationary phase approximation [27], because it is not exact (if we ignore δD), but it relies on the "smoothness" of the potential. However its application is much more straightforward, since it requires neither evaluations of determinants nor searches for stationary points, which may become prohibitive for high-dimensional integrals (we shall encounter a concrete example in the next chapter).

Chapter 5
A Model Problem

In Chapter 3, we have derived an exact expression for the dynamic response of a non-relativistic many-body system. We have used a path integral representation of the time evolution operator and have chosen a reference path as suggested by the physics of the problem we want to address, namely the approach to scaling. Indeed, we were able to derive, in a straightforward way, the scaling form of the structure factor at high momentum transfers and the $O(1/q)$ correction to scaling; both expressions are well known, and have been derived by different means by other authors.

In view of the generality of the path integral method, one expects it to be of some help in those cases in which the nature of the interactions or the experimental data available require more than simple perturbative expansions. However, while there exist well established techniques for computing with path integrals in imaginary time, only recently have people turned to dynamics problems requiring the evaluation of path integrals in real time. We have seen in Chapter 4 that the SPMC method offers some promises, especially when the relevant time scales in the problem are small; however, more work is clearly needed in that direction. In fact, not only do we lack a general technique, but we are not even aware of any attempt made at solving realistic problems.

5.1 The Exact Solution

It is important to test the SPMC method by solving model problems, for which an exact solution is available either analytically or by numerical quadrature. This is the case for the one-body problem, and also for the two-body problem, where the center-of-mass motion is separable. Here we show how the calculation of the structure factor is essentially reduced to computing the ground state and two scattering eigenstates of the Schrödinger equation. Let us consider a quantum system in the ground state $|\psi_0\rangle$, such that

$$H|\psi_0\rangle = E_0|\psi_0\rangle\,. \tag{5.1}$$

According to Eq. 3.12, we write the response as

$$\begin{aligned} S(\vec{q},\omega) &= \frac{1}{2\pi N}\int dt e^{i\omega t}\langle\psi_0|e^{iHt}\rho_{-\vec{q}}e^{-iHt}\rho_{\vec{q}}|\psi_0\rangle \\ &= \frac{1}{2\pi N}\int dt e^{i(\omega+E_0)t}\langle\psi_0|\rho_{-\vec{q}}e^{-iHt}\rho_{\vec{q}}|\psi_0\rangle\,. \end{aligned} \tag{5.2}$$

Now insert complete sets of position eigenstates and express the resulting propagator in terms of the retarded and advanced Green's functions [28]

$$K(x',x;t) = i(G^+(x',x;t)\theta(t) + G^-(x',x;t)\theta(-t))\,, \tag{5.3}$$

to obtain

$$\int dt e^{i(\omega+E_0)t}K(x',x;t) = 2i\mathrm{Im}G^+(x',x;\omega+E_0)\,, \tag{5.4}$$

whence

$$S(q,\omega) = -\frac{1}{\pi}\int dx dx' \psi_0(x)\psi_0^*(x')e^{-iq\cdot(x-x')}\mathrm{Im}G^+(x',x;\omega+E_0). \tag{5.5}$$

Let us start from the one-dimensional case. Again we work with unit mass for convenience. The retarded Green's function satisfies the inhomogeneous Schrödinger equation

$$\Big(\frac{d^2}{dx^2} + k^2 - 2V(x)\Big)G^+(x', x; k^2/2) = 2\delta(x - x')\,, \tag{5.6}$$

whose homogeneous associate is of the Sturm-Liouville type [29]. The boundary conditions simply require that G^+ be the outgoing Green's function:

$$G^+ \sim e^{\pm ikx}, \quad x \to \pm\infty.$$

Let $x_{>(<)}$ denote the greater (smaller) of x, x', and $\psi_{>(<)}$ be two outgoing solutions to the homogeneous equation, such that

$$\psi_>(x) \sim e^{ikx} \quad x \to \infty$$
$$\psi_<(x) \sim e^{-ikx} \quad x \to -\infty.$$

Then we have [30]

$$G^+(x', x; k^2/2) = \frac{2}{W(\psi_<, \psi_>)}\psi_<(x_<)\psi_>(x_>)\,, \tag{5.7}$$

where the Wronskian

$$W(\psi_<, \psi_>) = \Big(\frac{d}{dx}\psi_>(x)\Big)\psi_<(x) - \Big(\frac{d}{dx}\psi_<(x)\Big)\psi_>(x) \equiv \text{constant}\,, \tag{5.8}$$

is a function of $k \equiv \sqrt{2(\omega + E_0)}$. This shows that we only need to compute the ground state and two scattering states of the potential $V(x)$ to calculate the response function.

In three dimensions, with a central potential, we can still exploit the simple result of the Sturm-Liouville problem, after a partial-wave decomposition. We write

$$G^+(\vec{r'},\vec{r};k^2/2)=\sum_{l=0}^{\infty}\sum_{m=-l}^{l}\frac{g_l^+(r',r;k^2/2)}{rr'}Y_l^{*m}(\hat{r'})Y_l^m(\hat{r})\,, \tag{5.9}$$

where the Y's are spherical harmonics and g^+ is the solution to the inhomogeneous radial Schrödinger equation

$$\Big(\frac{d^2}{dr^2}+k^2-2V(r)-l(l+1)/r^2\Big)g_l^+(r',r;k^2/2)=2\delta(r-r')/r^2\,, \tag{5.10}$$

with the boundary conditions

$$g_l^+\sim e^{ikr},\qquad r\to\infty$$
$$g_l^+\sim r^l,\qquad r\to 0\,.$$

Denoting by u_l, v_l the solutions to the radial equation that are regular at the origin and outgoing at infinity, respectively, we have

$$g_l^+(r',r;k^2/2)=\frac{2}{W(u,v)}u_l(r_<)v_l(r_>)\,. \tag{5.11}$$

The response is now computed by substituting G^+ into Eq. 5.5, taking a spherically symmetric ground state, and using the identity

$$e^{i\vec{q}\cdot\vec{r}}=4\pi\sum_{l=0}^{\infty}\sum_{m=-l}^{l}i^l j_l(qr)Y_l^{*m}(\hat{q})Y_l^m(\hat{r})\,, \tag{5.12}$$

where j_l are the spherical Bessel functions of the first kind. The angular integrations are now trivial and one finds

$$\begin{aligned}S(q,\omega)=-4\int dr dr'\,rr'\psi_0(r)\psi_0(r')\sum_l j_l(qr)j_l(qr')(2l+1)\\ \times\,\mathrm{Im}\Big(\frac{2}{W(u,v)}u_l(r_<)v_l(r_>)\Big)\,.\end{aligned} \tag{5.13}$$

Again all we need is the ground state wave-function and two scattering states for each partial wave. In practice, computation is possible because only a finite number of partial waves contribute to the infinite sum. This results from the behavior of the regular Bessel functions at the origin and from the finite range, R, of the ground-state wavefunction:

$$j_l(qr) \sim (qr)^l\,, \qquad r \to 0\,,$$

so that

$$l \leq l_{max} \sim qR\,.$$

We are now ready to look at the details of the computation. As we simply want to test the principles of our method, we choose a finite attractive well,

$$V(r) = -V_0 \cosh^{-2}(r). \tag{5.14}$$

This potential lacks an important feature, displayed by atomic and nuclear potentials, namely a strong short-distance repulsive component. We shall address this problem in the next chapter.

The Schrödinger equation is integrated numerically using the fourth order Numerov algorithm [31]. Incidentally, we remark that the eigenstates are known in one dimension [32], being linear combinations of the associated Legendre functions [33]. This provides a check of the numerical solution. Once we have found the ground state and the retarded Green's function, Eq. 5.13 can be integrated using either some quadrature rule (we used Simpson's rule), or simply the Monte Carlo method. In the latter case, the ground state density matrix $\varrho(x', x) = \psi_0(x)\psi_0(x')$ is used as a weight, and ground state configurations are generated using the Metropolis algorithm [34].

5.2 The SPMC Calculation

The dynamic response was written exactly in Chapter 3 as the ground state average of the response operator (Eq. 3.13); the latter was in turn expressed as a real-time path integral (Eq. 3.18). The ground state average is computed by Monte Carlo, as discussed in Sec. 4.1.

Next we consider Eq. 3.18. The path integrals are carried out, as usual, by keeping a finite number of modes in the Fourier representation of the paths and discretizing commensurately the time integrals of the potential:

$$\begin{aligned}
&\int_0^0 \mathcal{D}\vec{\zeta}_+ \, \mathcal{D}\vec{\zeta}_- \, e^{i(S_+(\vec{\zeta}_+,\dot{\vec{\zeta}}_+,t)-S_-(\vec{\zeta}_-,\dot{\vec{\zeta}}_-,t))} \\
&= \int \frac{d^M\vec{\eta}_+ d^M\vec{\eta}_-}{(2\pi)^M} \exp\Big(i\mathrm{sgn}(t) \sum_{m=1}^{M} \tfrac{1}{2}(\vec{\eta}_m^+)^2/2 - it/(M+1) \sum_{j=1}^{M+1} V_{+j} \\
&\qquad - i\mathrm{sgn}(t) \sum_{m=1}^{M} \tfrac{1}{2}(\vec{\eta}_m^-)^2/2 + it/(M+1) \sum_{j=1}^{M+1} V_{-j} \Big) ,
\end{aligned} \tag{5.15}$$

where $\vec{\zeta}_0 = \vec{\zeta}_{M+1} = 0$. M modes are needed for $M+1$ timeslices; m numbers the modes, and j the timeslices. Otherwise, the notation is that used in Chapter 3. We write down the argument of the potential explicitly, for the 3D case:

$$\begin{aligned}
V_{+j} = V\Big(&\vec{z}_j^{\,+}(\{\vec{\eta}^{\,+}\}) + ((\omega/q^2)(x-x')_\parallel(\tilde{\kappa}+1)(\tilde{\xi}-1) - (x-x')_\parallel/2)\sigma\hat{q} \\
&+ \vec{x} - (\vec{x}-\vec{x}')_\perp\sigma/2 + \vec{v}_\perp(x-x')_\parallel/q(\tilde{\xi}-1)\sigma \Big)
\end{aligned} \tag{5.16}$$

$$\begin{aligned}
V_{-j} = V\Big(&\vec{z}_j^{\,-}(\{\vec{\eta}^{\,-}\}) + ((\omega/q^2)(x-x')_\parallel(\tilde{\kappa}+1)(\tilde{\xi}-1) + (x-x')_\parallel/2)\sigma\hat{q} \\
&+ \vec{x} + (\vec{x}-\vec{x}')_\perp\sigma/2 + \vec{v}_\perp(x-x')_\parallel/q(\tilde{\xi}-1)\sigma \Big) ,
\end{aligned} \tag{5.17}$$

with $\hat{q} \equiv \vec{q}/q$, $\vec{z} = \vec{\zeta}\sqrt{|t|}$, $\vec{\zeta}$ and $\vec{\eta}$ are related by a sine transform.

These expressions, together with the κ, ξ integrals, result in a $6M+2$ dimensional oscillatory integral, whose phase reduces to a quadratic form as $t \to 0$. We treat it by SPMC, as explained in Chapter 4. To make the correspondence with the formulas derived in that section more straightforward, we chose to use a Fourier representation of the path. As for the choice of the SPMC parameter ϵ, we have used different values for the integrals over the "lightcone" variables κ, ξ than for the path integral. We will denote these by ϵ_l and ϵ_x, respectively.

A different treatment is required in carrying out the integral over the transverse velocities, $\vec{v}_\perp$, which arises whenever there is more than one particle in the system or the spatial dimension is greater than one. The $t \to 0$ limit of the phase is linear in $v_\perp$: this indicates that the SPMC method is not suitable for this case, because there are no stationary points. However, in the same limit, the integral yields a δ-function in the transverse coordinates of the density matrix. This suggests that a good way of proceeding is to expand the potential through second order in $\vec{v}_\perp$ and do the resulting gaussian integral analytically, thus obtaining a quadratic phase in $(\vec{x} - \vec{x}')_\perp$. Note that, doing so, we are neglecting terms of order $1/q^4$ in the phase; therefore we expect the resulting approximation to be very accurate.

At this stage, we have gained some insight in the calculation. Only very small values of $(\vec{x}-\vec{x}')_\perp$ contribute constructively to the integral, i.e., $|(\vec{x}-\vec{x}')_\perp| \ll (x-x')_\parallel$. This means that it would be inefficient to generate $\vec{x}$, $\vec{x}'$ from the density matrix, which is isotropic. Instead, we take advantage of the new quadratic phase in $(\vec{x}-\vec{x}')_\perp$ and generate values of $(\vec{x} - \vec{x}')_\perp$ by SPMC, obtaining a narrow gaussian distribution around zero at high q. The density matrix is used to generate $(\vec{x} + \vec{x}')$ as well as $(x - x')_\parallel$ via the Metropolis algorithm. It is amusing (but perhaps not surprising!) to note that the normalization of this weight is now $2\pi q\, S_{IA}(Y = 0)$.

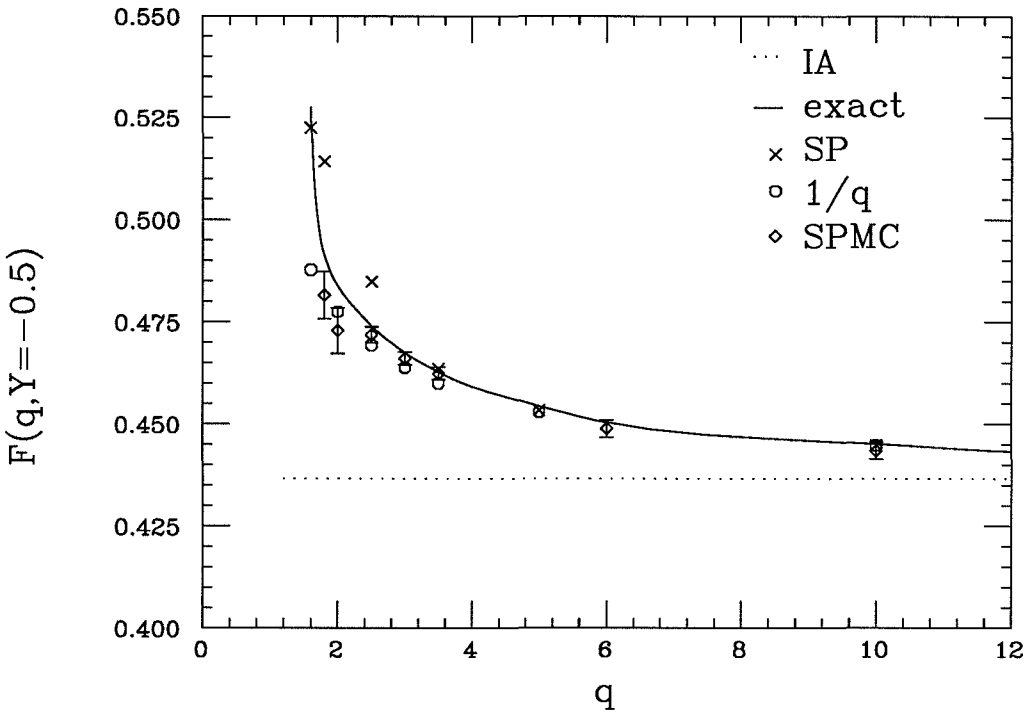

Figure 5.1 – $F(q,Y)$ as a function of q at fixed $Y = -0.5$ for a particle in the $1D$ potential well $V(x) = -0.8\cosh^{-2}x$. In our units, $\hbar = m = 1$. The ground state energy is $E_0 = -0.37$; the minimum allowed momentum transfer is $q_0 = 1.5$. Here and in the remaining figures we plot $\pm 1\sigma$ error bars.

We have calculated the QE response for a particle in the 1D well $V(x) = 0.8\cosh^{-2}(x)$ and in the 3D spherical well $V(r) = 21\cosh^{-2}(r)$. The potential sets the length scale, and hence the momentum scale. The ground state energies are respectively $E_0 = -0.36$ and $E_0 = -12.5$. For any given Y, the requirement that the struck particle be excited to the continuum (i.e., that $\omega > -E_0$), fixes a minimum value for the momentum transfer:

$$q > q_0 = -Y + \sqrt{Y^2 - 2E_0}. \tag{5.18}$$

The time scale of the problem is set by the ratio $\langle |x - x'| \rangle_{\|}/q$. If the product of this number and the average value of the potential is smaller than one, one can regard the

time scale as "small," and the intuitive arguments at the end of Sec. I apply. However, as the product approaches one, we expect the SPMC method, as formulated in the present paper, to break down. This will clearly happen for very strong potentials at any q, and for weak potentials near $q \simeq q_0$. For our potentials, this happens around $q \lesssim 2$ in 1D and $q < 10$ in 3D. For nuclear interactions, considering the attractive part of the potential only, one estimates that SPMC breaks down at momentum transfers smaller than 1 GeV/c.

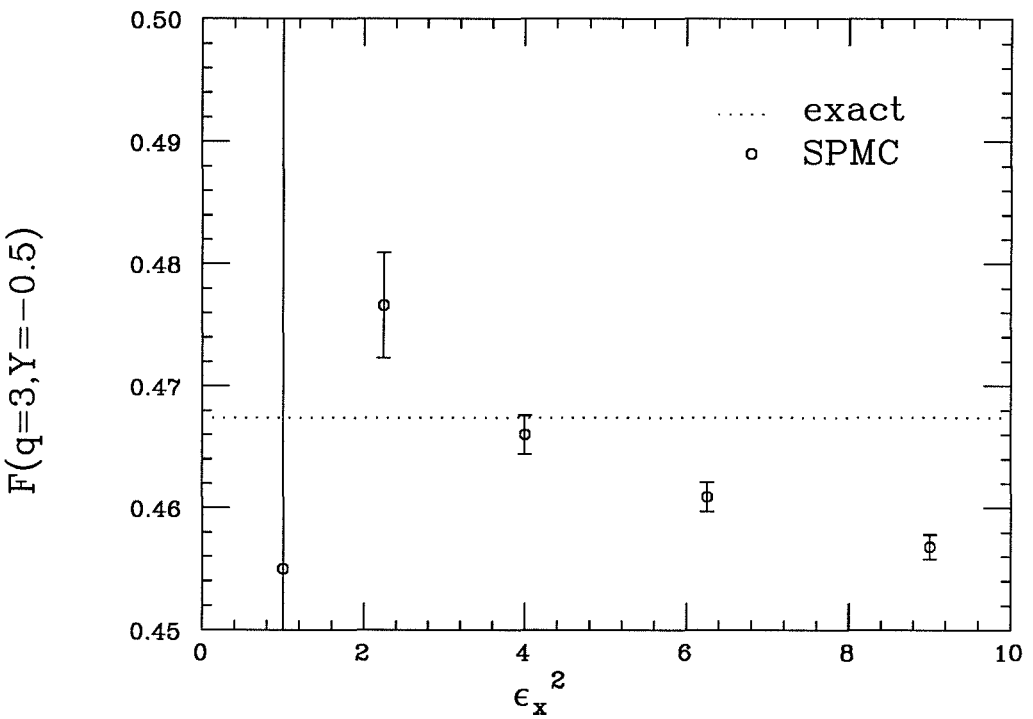

Figure 5.2 – $F(q = 3, Y = -0.5)$ as a function of the SPMC parameter ϵ_x^2 ($\epsilon_l = 1$). The potential is the same as in Fig. 5.1.

For the particle in 1D, we have calculated the QE response at fixed $Y = -0.5$ for all the allowed values of q. In Fig. 5.1, we plot $F^i(q, Y)$ vs. q and compare it to the exact result (solid line) as well as to the IA, which is a constant. We have also

performed the real time integrals (5.15) by the stationary phase (SP) method [27] and plot the results for comparison. The time integrals were carried out on a 16 point grid (i.e., we keep 15 Fourier modes). The SPMC parameters were chosen to be $\epsilon_l = 1$ and $\epsilon_x = 2$. We have checked the ϵ dependence of the results by calculating at different ϵ_x and ϵ_l. In Fig. 5.2 we plot the scaled response $F(q = 3, Y = -0.5)$ with $\epsilon_l = 1$ for different values of ϵ_x. We can see how the statistical errors decrease dramatically moving up from $\epsilon_x = 1$. At higher values (i.e., $\epsilon_x \simeq 2.5$), a larger systematic error sets in, which should be attributed to the fact that we are ignoring the correction δD in our calculation.

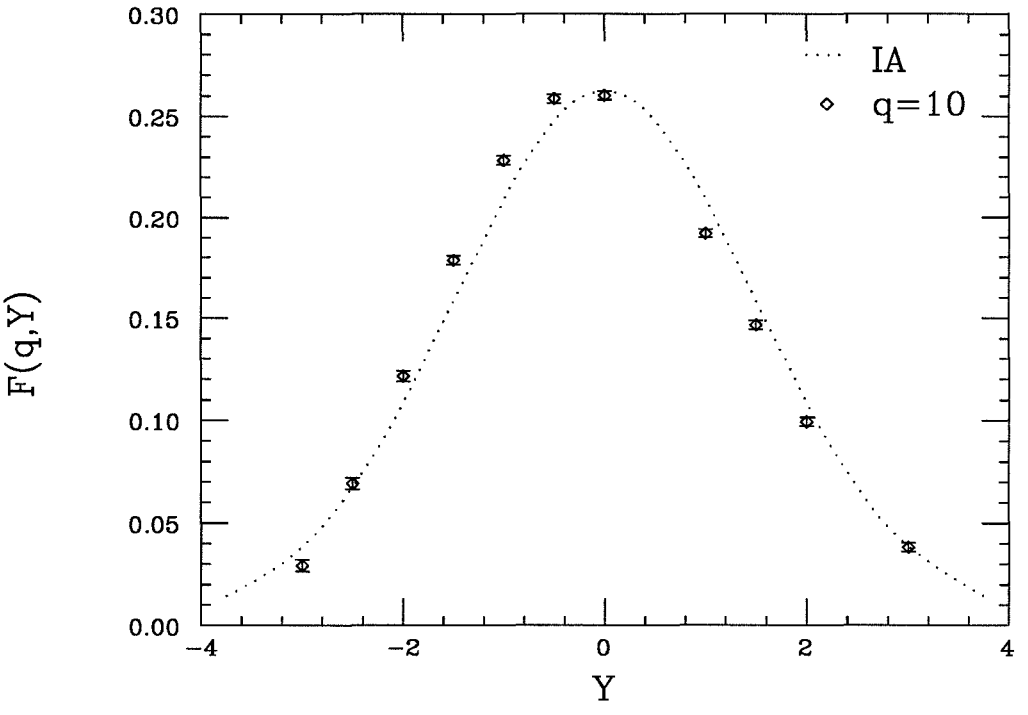

Figure 5.3 – $F(q,Y)$ as a function of Y at fixed $q = 10$ for a particle in the $3D$ spherical well $V(r) = -21\cosh^{-2} r$. The ground state energy is $E_0 = -12.5$. The scaling limit (which for our potential coincides with the IA) is reached at about $q = 40$, within our error bars (see also Fig. 5.5).

Next we present results for the particle in the 3D potential well. In Fig. 5.3 we plot $F^i(q,Y)$ at fixed $q = 10$ as a function of Y. We kept 15 Fourier modes and checked for convergence with 23 modes at $Y = -0.5$. The dimension of the oscillatory integral, in this case, was 140. The SPMC parameters were chosen to be $\epsilon_l = 1$ and $\epsilon_x = 2.2$. We notice that the peak of the curve is shifted towards negative Y, with respect to the IA. It is known that this is the case when we are dealing with smooth, attractive interactions, because the deviations from the IA are best described by the $O(1/q)$ correction (Eq. 3.24), which is odd in Y.

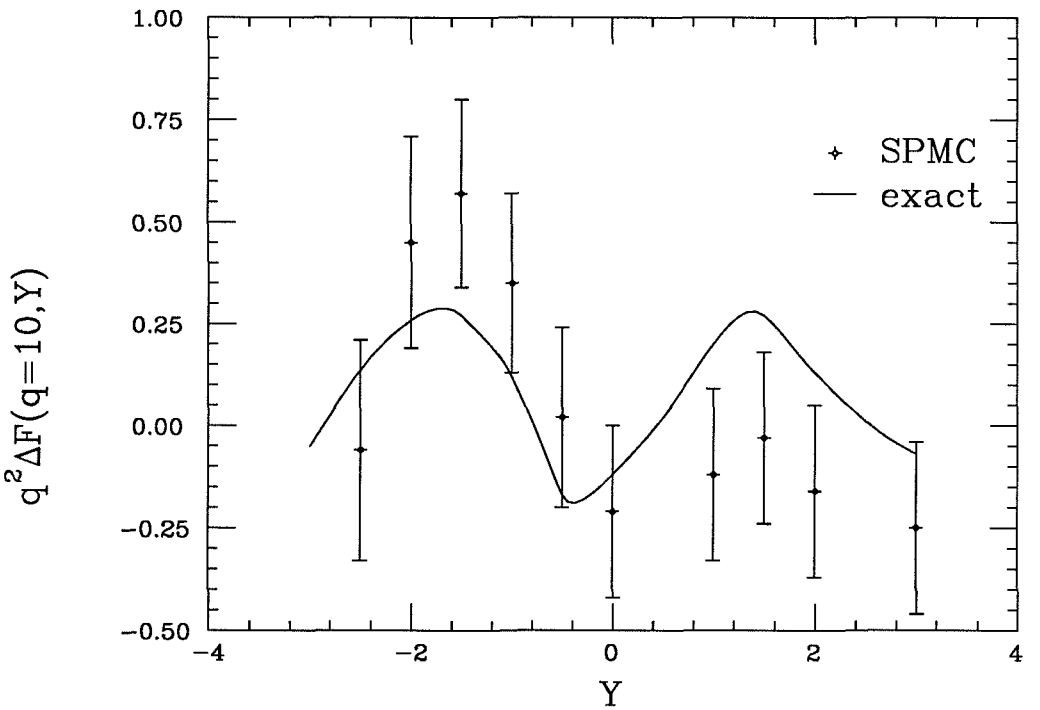

Figure 5.4 – Contributions $O(1/q^2)$ and higher to $F(q,Y)$ as a function of Y at fixed $q = 10$ (same potential as Fig. 5.3). The q dependence was eliminated in lowest order by subtracting the IA and the $O(1/q)$ contribution (see Eq. 3.24) and multiplying through by $q^2 = 100$.

If one regards the one-body problem as describing a two-body system in the center of mass, it is sensible to define the coherent response, according to Eq. 3.25. Exact calculations show that the coherent response, $F^c(q,Y)$, is suppressed by about a factor $10^2 \sim 10^3$ with respect to $F^i(q,Y)$, which makes it impossible to carry out a meaningful SPMC calculation, given our error bars.

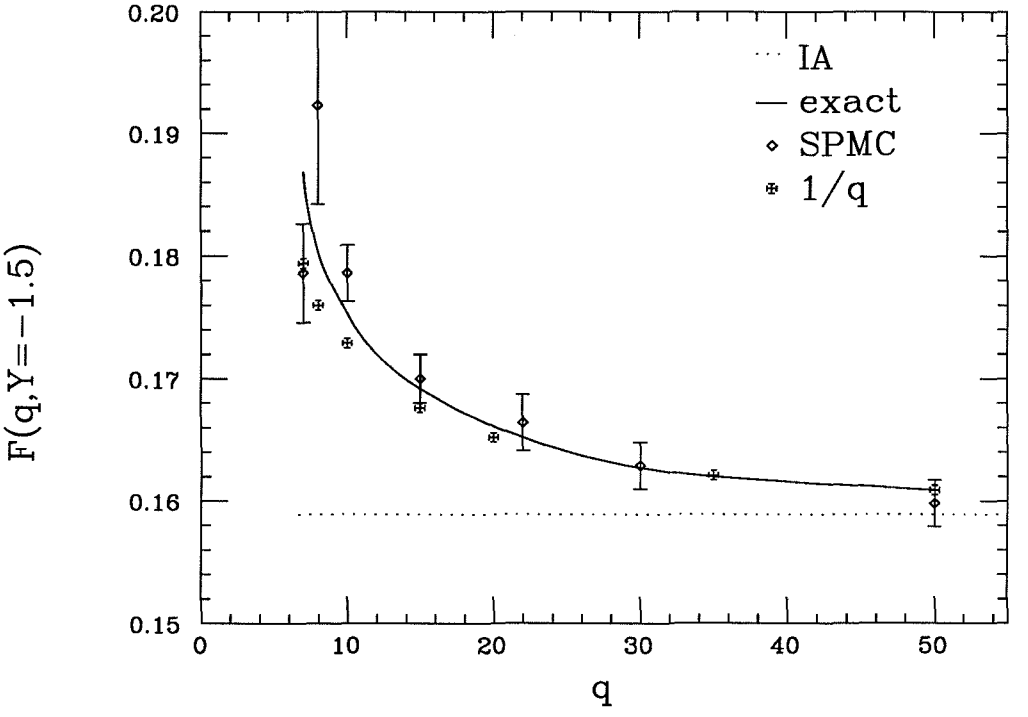

Figure 5.5 – $F(q,Y)$ as a function of q at fixed $Y = -1.5$. The potential is the same as in Fig. 5.3. The minimum allowed momentum transfer is $q_0 = 6.72$.

In Fig. 5.4 we plot the difference between the scaled response function $F(q,Y)$ and its value through order $1/q$, which can be calculated reliably (i.e., without the complications introduced by the real time dynamics) using Eq. 3.24. It is no surprise that this quantity is very small. Indeed, as we pointed out before, Eq. 3.24 works

remarkably well for smooth interactions. The results are multiplied by $q^2 = 100$, since they are expected to be $O(1/q^2)$.

In Fig. 5.5 we plot $F(q, Y)$ at fixed $Y = -1.5$. The "exact" result is obtained as described in Sec. 5.1, for $q < 20$, and joined smoothly to the "exactly" known $1/q$ correction for large q, where the numerical integration of the Schrödinger equation starts to become problematic. Again, the SPMC calculation was performed with 15 modes and checked the result at $q = 15$ with 23 modes. The SPMC parameters are the same we chose for Fig. 5.3. We can see that the SPMC gives a satisfactory answer down to $q \sim 10$. Below that, the errors become large. The reason is that we are not including the derivatives of the potential in our sampling weight (i.e., our weight is given by Eq. 4.22 instead of Eq. 4.20); this works satisfactorily at high q, because the derivatives of the potential are all suppressed by $1/\sqrt{q}$. The lowest q for which we calculate, $q = 7$, is very close to the lowest allowed momentum transfer, $q_0 = 6.72$. We also point out that, although the strength of the potential, V_0, is much smaller in the 1D case than in 3D, the SPMC method in the latter case breaks down at relatively much lower values of q; we attribute this to the role played by the centrifugal force in three dimensions.

Chapter 6
Strong Interactions and Hard Cores

In the previous chapters, we have discussed the QE response of a non-relativistic many-body system in the high momentum transfer limit. We have formulated the response in a way that separates the final state (dynamic) properties from those of the initial state (static). This allowed us to establish Y-scaling for finite many-body interactions, where the short time propagator tends to the free propagator as $t \to 0$. We were able to recover the simple expression of the $O(1/q)$ scaling violations first obtained by Gersch *et al.* [9] using a different approach.

However, Gersch's theory is not suitable for calculations involving strong interactions. This affects its capabilities of making predictions about real many-body systems, whose interparticle potential usually consists of a strong repulsive core at short range and a weak attractive tail at large distance. The path integral method clearly suggests how to proceed in this case. Indeed, we recall that the potential was explicitly introduced in Eq. 3.6, but one need not do so. Instead, the propagator can be rewritten exactly as a convolution of short time propagators:

$$\langle x'|e^{-iHt}|x\rangle = \int dx_1 \cdots dx_{N-1} \langle x'|e^{-iHt/N}|x_1\rangle \cdots \langle x_{N-1}|e^{-iHt/N}|x\rangle \ . \qquad (6.1)$$

If N is chosen large enough that in the time interval t/N only binary interactions are important, then the short time propagators can be written as products of two-body terms [35], which are the Fourier transforms of the two-body Green's function for the strong potential. Our goal in this chapter is to carry out this program for

a soft core nucleon-nucleon interaction to be used subsequently, the Malfliet-Tjon potential. This is a two-yukawa potential, whose singularity at the origin is of the Coulomb type $(1/r)$. Therefore, we will have to calculate the exact propagator for the Coulomb interaction. Then we will show what modifications would be required to deal with rigorously hard core potentials.

6.1 The Exact Two-Body Propagator

In this section, we show how the two-body propagator

$$K(\vec{x}_1', \vec{x}_2', \vec{x}_1, \vec{x}_2; t) \equiv < \vec{x}_1', \vec{x}_2' | e^{-iHt} | \vec{x}_1, \vec{x}_2 > \tag{6.2}$$

can be calculated exactly from the eigenstates of the two-body hamiltonian

$$H = -\frac{1}{2m}\left(\frac{d^2}{d\vec{x}_1} + \frac{d^2}{d\vec{x}_2}\right) + V(|\vec{x}_1 - \vec{x}_2|)\,. \tag{6.3}$$

It is convenient to shift to center-of-mass coordinates,

$$\begin{aligned} \vec{X} &\equiv (\vec{x}_1 + \vec{x}_2)/2 \\ \vec{x} &\equiv \vec{x}_1 - \vec{x}_2\,, \end{aligned} \tag{6.4}$$

where the problem is separable:

$$\begin{aligned} K(\vec{x}_1', \vec{x}_2', \vec{x}_1, \vec{x}_2; t) &\equiv K(\vec{X}', \vec{X}; t)\, K(\vec{x}', \vec{x}; t) \\ K(\vec{X}', \vec{X}; t) &= \frac{1}{(\pi i t/m)^{3/2}} e^{i(\vec{X}' - \vec{X})^2/4m} \\ K(\vec{x}', \vec{x}; t) &= < \vec{x}' | e^{-it(p^2/m + V)} | \vec{x} >\,, \end{aligned} \tag{6.5}$$

Here p is the momentum of the relative motion, and the center-of-mass propagates according to the free dynamics. The propagator of the relative motion is non-trivial,

and can be calculated following closely the discussion of Sec. 5.1. We start out observing that the unitarity of the time-evolution operator, expressed by the identity

$$K(\vec{x}', \vec{x}; t) = K^*(\vec{x}, \vec{x}'; -t)\,, \tag{6.6}$$

allows us to consider propagation forward in time without loss of generality. Therefore, in the remainder of this section, we assume $t \geq 0$, so that the propagator is given, up to a factor i, by the retarded Green's function [28]

$$K(\vec{x}', \vec{x}; t) \equiv iG^+(\vec{x}', \vec{x}; t)\,. \tag{6.7}$$

Furthermore, we observe that for central potentials, the propagator can depend only on x', x, and θ, so we can expand it in Legendre polynomials in the following fashion:

$$K(\vec{x}', \vec{x}; t) = \sum_{l=0}^{\infty} \frac{2l+1}{4\pi} P_l(\cos\theta) K_l(x', x; t)\,. \tag{6.8}$$

Upon inverting Eq. 5.4, we obtain

$$K_l(x', x; t) = -2 \int_0^{\infty} \frac{d\omega}{2\pi} \mathrm{Im} G_l^+(x', x; \omega) e^{-i\omega t}\,. \tag{6.9}$$

This corresponds to integrating the discontinuity of G_l along the $\omega > 0$ cut. This is all, if the potential doesn't have any bound state, as in the case, for example, of a repulsive Coulomb interaction. If we had bound states, i.e., if G_l had poles on the negative ω axis, they would contribute a discrete sum, $\sum_n \exp(-i\omega_n t)\psi_{n,l}(x)\psi^*_{n,l}(x')$ to the right hand side.

In this way, the calculation of the exact two body propagator reduces to that of the retarded Green's function for the center-of-mass problem, which was solved in Sec. 5.1. This allows us to define an effective potential through the relation

$$K(\vec{x}', \vec{x}; t) \equiv K_{free}(\vec{x}', \vec{x}; t) e^{-itV_{eff}(x', x, \cos(\theta); t)}\,. \tag{6.10}$$

Thus, the effective potential,

$$V_{eff} = \log\Big((4\pi it/m)^{3/2} e^{-im(\vec{x}'-\vec{x})^2/4t} K(\vec{x}', \vec{x}; t)\Big) \tag{6.11}$$

will in general be a non-local, complex function of $\vec{x}'$, $\vec{x}$, and also of time.

6.2 The Nucleon-Nucleon Interaction

As the nucleon-nucleon interaction, we choose the Malfliet-Tjon (MT) potential (Fig. 6.1) [36]. This is a spin-independent central potential, obtained by fitting the sum of two Yukawa potentials to low energy ($\leq$ 300 MeV) parameters (e.g, the scattering phase shifts). Several slightly different sets of parameters can be obtained through such fits, but the choice among them is quite an irrelevant issue for our purpose. Our units are such that

$$\hbar = 1$$

$$c = 1$$

$$m_n = 2$$

(observe that now the reduced mass is unity). Thus the potential takes on the following form:

$$V(r) = \frac{1}{r} \times (7.39e^{-1.3062r} - 3.22e^{0.6531r}), \tag{6.12}$$

where the unit energy is 469.5 MeV and the unit length is 0.42 fm. For comparison, we write down the Coulomb potential between two protons:

$$V_C = 0.007297 \times \frac{1}{r}, \tag{6.13}$$

which can be regarded as a small perturbation.

While in principle our program of calculating the exact two-body propagator can be carried out for the full MT potential, following the steps outlined above and in Sec. 5.1, it is more convenient to split the potential into a regular (V_r) and a singular (V_s) part. These are displayed in Fig. 6.2. We observe that this decomposition yields

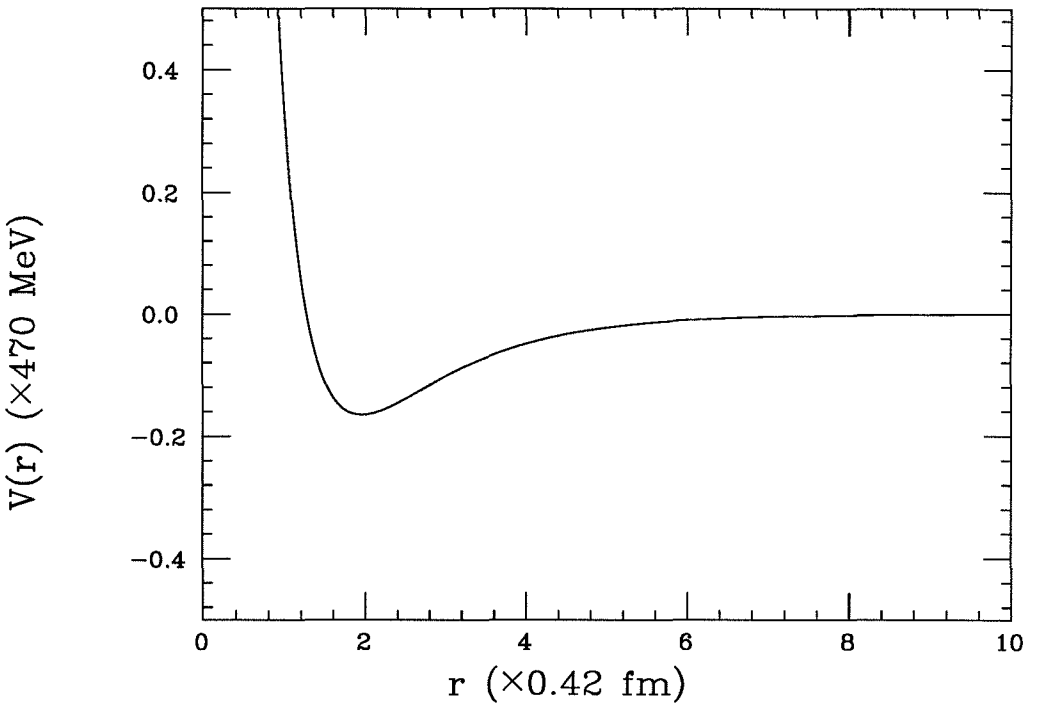

Figure 6.1 – The nucleon-nucleon Malfliet-Tjon potential, assumed to act in all states.

a purely attractive regular component, and the repulsive core is completely absorbed in the singular part. Because the latter is of the Coulomb type,

$$V_s(r) = \frac{\alpha}{r}\,, \tag{6.14}$$

with $\alpha = 4.17$, its eigenstates are known [37] (i.e., they can be calculated efficiently without having to integrate the Schrödinger equation numerically). Here we give the details of the calculation of the Coulomb propagator. After the usual partial wave decomposition, the radial Schrödinger equation becomes

$$\Big(\frac{d^2}{d\rho^2} + 1 - \frac{2\eta}{\rho} - \frac{l(l+1)}{\rho^2}\Big)\varphi_l(\rho) = 0\,,$$

where

$$\rho = kr$$

$$\eta = \alpha/k\,.$$

The general solution is a linear combination of the regular and irregular solutions at the origin, denoted by $F_l(\eta,\rho)$ and $G_l(\eta,\rho)$, respectively. These are normalized to have unit Wronskian:

$$W(F_l, G_l) = -1.$$

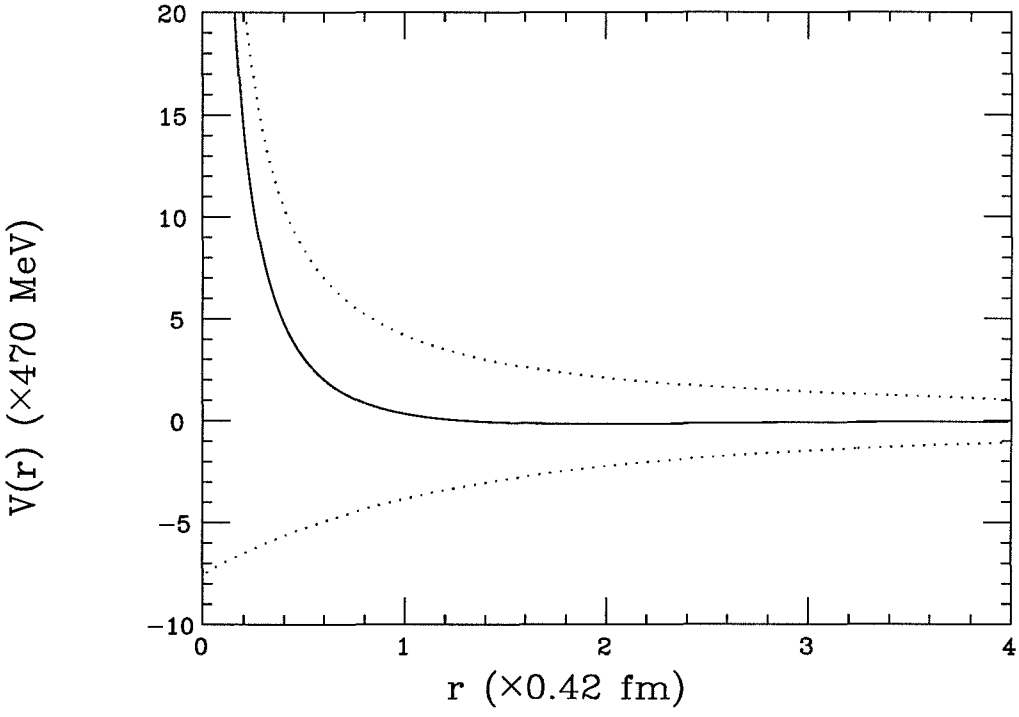

Figure 6.2 – The nucleon-nucleon potential of Fig. 6.1 (solid line), decomposed into regular and singular ($1/r$) terms (dotted lines).

The first step is to construct the outgoing Green's function. To this end, we observe that

$$G_l + iF_l \sim e^{i(\rho - \eta \log 2\rho)} \sim e^{i\rho}$$

as $\rho \to \infty$; this provides the required outgoing wave function. Therefore, we write

$$g_l^+(r', r; \omega = k^2/2) = -\frac{2}{kr_< r_>} F_l(\eta, kr_<)(G_l(\eta, kr_>) + iF(\eta, kr_>)) , \qquad (6.15)$$

whereupon the l-th wave Coulomb propagator is obtained by the following integration

$$K_l(r', r; t) = \frac{1}{\pi} \int_0^\infty d\omega e^{-i\omega t} 2F_l(\eta, kr') F_l(\eta, kr)/k . \qquad (6.16)$$

Adding the contributions of all partial waves, we arrive at the propagator for the singular part of the MT potential,

$$K_s(\vec{x}', \vec{x}; t) \equiv < \vec{x}' | e^{-it(P^2/2 + V_s)} | \vec{x} > .$$

The full propagator is then obtained simply in the following fashion:

$$K(\vec{x}', \vec{x}; t) = K_s(\vec{x}', \vec{x}; t)\, e^{-itV_r} . \qquad (6.17)$$

6.3 Storing the Propagator

We are now ready to look into the details of the actual computation. We are facing two main problems: one is carrying out the integral for the real-time propagator (Eq. 6.16), and the other one is storing the results efficiently. The solution to both problems clearly involves restricting the domain in space and time, where the procedure above needs to be carried out. A few considerations on Eq. 6.16 are required. The familiar free-particle expression (we recall that we work with reduced mass $\mu = 1$),

$$K_l^0(r', r; t) = \frac{4\pi}{(2\pi i t)^{3/2}} e^{i(r'^2+r^2)/2t}(-i)^l j_l(r'r/t) \tag{6.18}$$

is recovered for $\eta = 0$, i.e., for zero charge or for very high momentum (very short time). While this provides an essential check of the computer codes, here we are clearly interested in the strong coupling regime, where the naive semiclassical approximation, $K_l = K_l^0 e^{-itV}$, breaks down. In particular, we have to find the propagator for finite time and short distance (where the repulsion is strong). In this regime, we expect the propagator to be determined by the behavior of the regular Coulomb wavefunction for $\eta \gg \rho$, i.e., to be suppressed by the "penetration factor" $C(\eta)$ [37],

$$F_l^2 \propto C^2(\eta) = \frac{2\pi\eta}{(e^{2\pi\eta} - 1)}. \tag{6.19}$$

We begin by restricting the spatial domain of the calculation. For $r > 1$, $r' > 1$, the MT potential is so small that it can be treated in the usual way (Eq. 3.6). Instead, we calculate the exact propagator when both r, $r' < 1$. In this way, we are not comprising the potentially dangerous trajectories that reach deep into the core starting from far out. These occur frequently enough to require special treatment. So we carry out the exact calculation also in the domain $r < 0.6$ and $r' \leq 3$. We

also set a lower limit to r, by implementing a hard core requirement (i.e., $K = 0$) whenever r, $r' < 0.2$. Physically, this corresponds to distances $r < 0.08$ fm, so this approximation is certainly justified; numerically, one cannot see any difference in the calculated QE response (see next chapter) even if the lower cutoff is moved to $r = 0.4$.

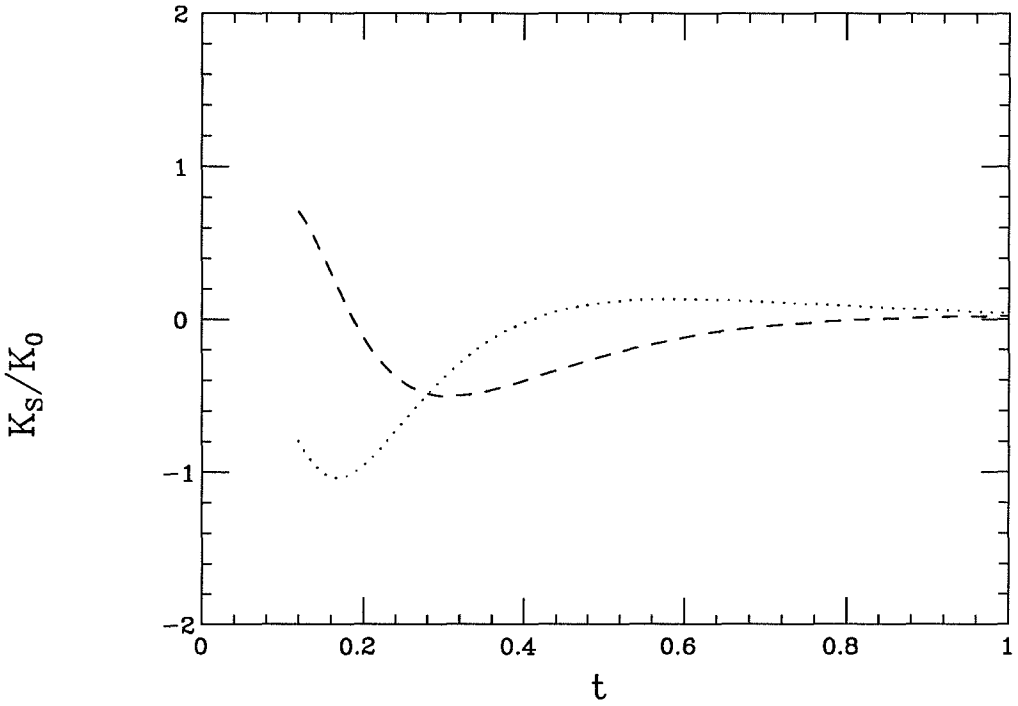

Figure 6.3 – Numerical computation of the exact "Coulomb" propagator (normalized to the free particle) at fixed $r = 0.4$, $r' = 0.8$, $\cos\theta = 1$, as a function of time (real part = dashed line, imaginary part = dotted line). The coupling constant is $\alpha = 4.17$.

It is particularly important that the calculation of the Coulomb propagator be cut off at some upper distance, because this effectively turns into an upper bound on the number of partial waves needed for convergence of Eq. 6.8. We find that $l \leq 10$ is usually sufficient. Of course, this would not be the case if we calculated for extremely short times (i.e., very high momenta), but we avoid that. This is

because a further complication occurs for very short times, that is, the energy Fourier transform is numerically ill-behaved. Fortunately, we can set a lower cut-off in time, $t = 0.2(rr')^{1/2}$, such that for shorter times $tV(r) < 1$ on average, and we are effectively dealing with a "weak" potential, and may use again Eq. 3.6. Finally, we find that for times $t > 2$ (i.e., for low momenta) the Coulomb barrier is effectively preventing propagation near the core, and again we can put $K = 0$. (Incidentally, one would not normally deal with such long timeslices in a path integral calculation; however, since the QE response is actually expressed as a time Fourier transform, our timeslice is actually a stochastic variable, and it can in principle happen, although extremely unlikely, that we have to evaluate the propagator for large t.)

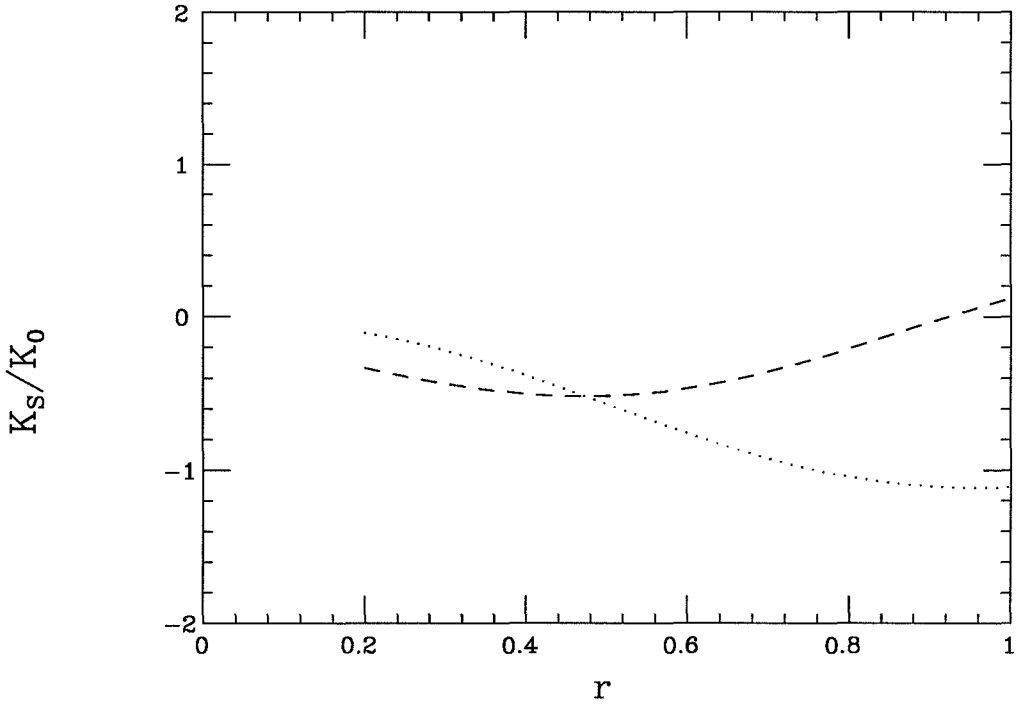

Figure 6.4 – Numerical computation of the exact "Coulomb" propagator (normalized to the free particle) at fixed $t = 0.3$, $r = 0.4$, $\cos\theta = 1$, as a function of penetration distance (real part = dashed line, imaginary part = dotted line).

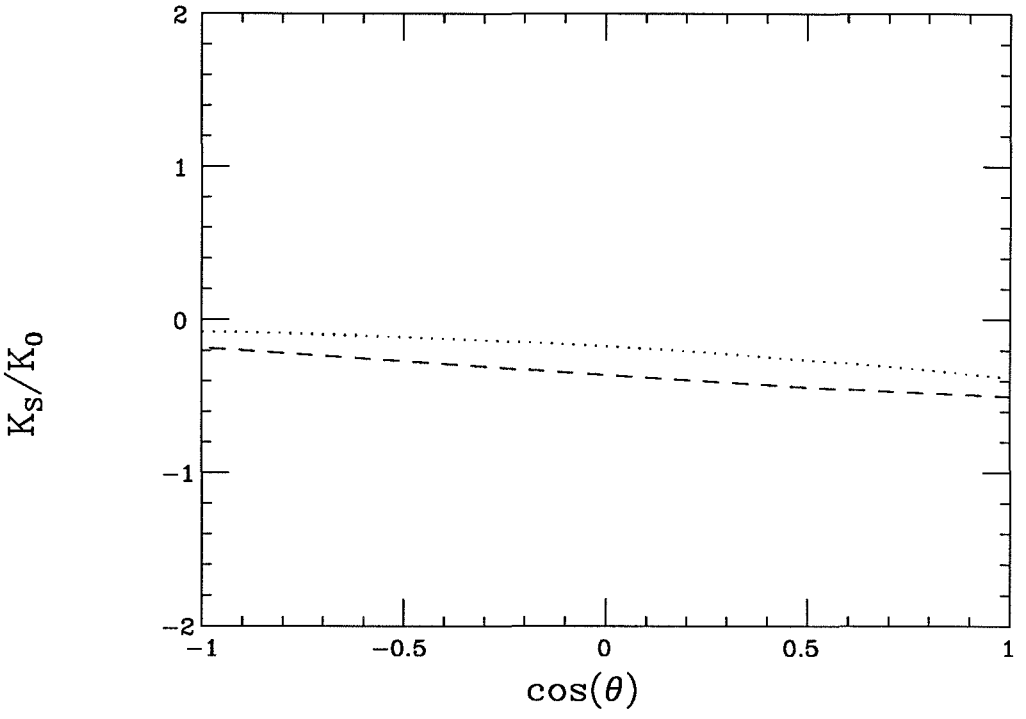

Figure 6.5 – Numerical computation of the exact "Coulomb" propagator (normalized to the free particle) at fixed $t = 0.3$, $r = 0.4$, $r' = 0.8$, as a function of the angle (real part = dashed line, imaginary part = dotted line).

The energy Fourier transform is carried out by an IMSL library integration routine. To get a feel for how the propagator looks like, we show a few plots of the ratio K_s/K_0. In Fig. 6.3, this is plotted at fixed $r = 0.4$, $r' = 0.8$ and $\cos\theta = 1.$, as a function of time. In Fig. 6.4, time is fixed ($t = 0.3$) and r is allowed to vary from 0.2 to 1. In Fig. 6.5, the ratio is plotted as a function of $\cos\theta$. In all cases, the propagator shows a very smooth behavior, which in turn translates into a smooth effective potential (except that the real part of the latter abruptly changes sign when the imaginary part of the former goes through zero). As a consequence, we need not store the effective potential on a very dense grid. We decided to store it as a

four-dimensional matrix,

$$V_{eff}(r_<, r_>, t, \cos\theta) \rightarrow V_{eff}(i, j, k, l).$$

The gridpoints are chosen homogeneously in radius (step $\Delta r = 0.1$) and solid angle (step $\Delta \cos\theta = 0.1$), whereas we chose a time step $\Delta t = 0.02$ for $t \leq 0.5$ and $\Delta t = 0.1$ for $t \geq 0.5$. In the actual calculation, we are required to evaluate V_{eff} at arbitrary point in space-time. We interpolate linearly between the stored values using a five-point Lagrange interpolation formula in four dimensions.

6.4 Scaling and Hard Cores

The hard core potential represents a very special type of strong interaction, because it can never be treated perturbatively with respect to the momentum transfer. Since such perturbative arguments are the key to the relation between the response function at high q and the momentum distribution through the Impulse Approximation, we may expect that additional complications arise for hard cores. Indeed, we shall show that the IA breaks down: the response does scale at high q, but the scaling function is not the momentum distribution, nor is it related to it by convolution with simple broadening functions, as postulated in Silver's "hard core perturbation theory" [15].

Of course, a perturbation parameter still exists; we must recover the free particle case as the core radius a goes to zero, or, equivalently, for vanishing density or infinite lengthscale of the density matrix. Thus, for dilute systems, we expect only binary collisions to be important, and we can proceed to regularize the two-body interaction as described earlier in this chapter. The two-body density matrix must vanish at (and inside) the core, and can be calculated in terms of spherical Bessel functions outside. Unfortunately, the time integration, Eq. 6.9, can only be done numerically.

However, in this discussion we are interested only in the infinite q limit. Here one can use the concepts of geometric optics, as is done in recent work by Gurvitz, Rinat and Rosenfelder [17]. We won't follow this strategy, but show how the same result can be arrived at using path integrals.

Following very closely the derivation of Sec. 3.2, we write the scaled response, F, in terms of the equilibrium density matrix and the response operator:

$$\begin{aligned} F(\vec{q},\omega) &= q\int dx\,dx'\,\varrho(x,x')\Omega(x',x) \\ &= \int dx\,dx'\,\varrho(x,x')\int\frac{dt}{2\pi N}\,e^{i\omega t}\sum_{i,j}\int dx_0\langle x'|e^{iHt}|x_0\rangle\langle x_0|e^{-iHt}|x\rangle\,e^{i\vec{q}\cdot(\vec{x}_i-\vec{x}_j^{\,0})}. \end{aligned} \tag{6.20}$$

Again we specialize to the incoherent response. We can carry out the very same coordinate changes as we did before, to arrive at (see Eq. 3.18)

$$\begin{aligned} F(\vec{q},\omega) = \frac{1}{2\pi}e^{-iY(x-x')_\parallel}\int\frac{d\kappa\,d\xi}{2\pi}\,e^{-i\kappa\xi}\int\frac{d^{n-1}v_\perp}{(2\pi)^{n-1}}\,e^{-iv(x-x')_\perp} \\ \times\frac{1}{(2\pi)^{N-1}}\int_0^0 d^{N-1}\zeta_{+j}\,d^{N-1}\zeta_{-j}\prod_{j=1}^{N}K_j(+)\prod_{j=1}^{N}K_j(-)\,. \end{aligned} \tag{6.21}$$

Using Eq. 3.19 (with an effective potential yet to be discussed), we write

$$K_j(\pm)\equiv e^{\pm\mathrm{sgn}(t)i(\zeta_{\pm j}-\zeta_{\pm j-1})^2/2\mp i(x-x')_\parallel/qN\,(\tilde{\xi}-1)V_{eff}(z_{\pm j},z_{\pm j-1};\tilde{\kappa},\tilde{\xi},v/q;x,x';j)} \tag{6.22}$$

where we recall that z, $\tilde{\kappa}$, $\tilde{\xi}$ are all suppressed by $1/\sqrt{q}$ with respect to ζ, κ, ξ, respectively. In this way, we can take the $q\to\infty$ limit, by evaluating the effective potential along the "eikonal" trajectories; however, unlike what was done in Eq. 3.23, here we may not expand the exponential in powers of V/q. The argument of the potential becomes

$$\begin{aligned} V_{eff}(+;j) &= V_{eff}(x-(x-x')_\parallel j/N) \\ V_{eff}(-;j) &= V_{eff}(x') \end{aligned} \tag{6.23}$$

and thus, as in Ch. 3, all integrals become trivial, yielding the scaling function

$$F(Y) = \frac{1}{2\pi}\int dx\, dx' \varrho(x,x') e^{-iY(x-x')}\delta^{n-1}(x-x')_\perp \\ \times \exp\Big(i(x-x')_\parallel/q \int_0^1 d\sigma (V_{eff}(x-(x-x')_\parallel\sigma) - V_{eff}(x'))\Big)\,. \tag{6.24}$$

The effective potential introduced here is simply a trick to implement the hard core boundary condition for the many-body Green's function, i.e., to make the latter vanish whenever any two (or more) particles touch. Therefore, it is a many-body interaction, taking on the value

$$V_{eff} = i\infty \mathrm{sgn}(x-x'),\ \text{if any two particles overlap} \\ = V_{reg},\ \ \text{otherwise.} \tag{6.25}$$

Of course, since we are taking the $q \to \infty$ limit, the regular part of the interaction should be taken to be zero. Observe that we may drop the term $V_{eff}(x')$ in the previous equation. This is legitimate, because there is no need to implement the hard core condition at x': the exact density matrix of the system, $\varrho(x,x')$ does this automatically.

The correction to the IA is simplest in the two-body problem (in the many-body case multiple scattering, i.e., multiple reflections, considerably complicate the calculation). Here Eq. 6.24 reduces to

$$F(Y) = \frac{1}{2\pi}\int d^2R_\perp\, dz dz' \varrho(\vec{R}_\perp, z; \vec{R}_\perp, z') \\ e^{-iY(z-z')} e^{i(z-z')/q \int_0^1 d\sigma\, V_{eff}\left(\vec{R}_\perp + (z-\sigma(z-z'))\hat{z}\right)}. \tag{6.26}$$

The hard core constraint will be effective for

$$|\vec{R}_\perp + (z-(z-z')\sigma)\hat{z}| \le a\,,\ 0 \le \sigma \le 1\,, \tag{6.27}$$

that is, for

$$\begin{aligned} |\vec{R}_\perp| &< a \\ zz' &< 0. \end{aligned} \tag{6.28}$$

Hence, the correction to the IA is given by

$$\begin{aligned} \Delta F(Y) &\equiv F(Y) - F_{IA}(Y) \\ &= \frac{1}{2\pi} \int d^2R_\perp \, dz dz' \varrho(\vec{R}_\perp, z; \vec{R}_\perp, z') e^{-iY(z-z')} \\ &\qquad \times \left(1 - e^{i(z-zl)/q \int_0^1 d\sigma \, V_{eff}(\vec{R}_\perp + (z - \sigma(z-zl))\hat{z})}\right) \\ &= -2 \int_0^a dR_\perp \, R_\perp \int_{-\infty}^0 dz \int_0^\infty dz' \varrho(\vec{R}_\perp, z; \vec{R}_\perp, z') e^{-iY(z-zl)} \, . \end{aligned} \tag{6.29}$$

This expression has several noteworthy properties, that are maintained in the many-body case. First, it does Y-scale; this shows that in an experiment Y-scaling alone doesn't guarantee that the momentum distribution is being measured. This was first suggested by Weinstein and Negele [5], who nevertheless did not arrive at an exact analytical expression. Another interesting property is that ΔF is even in Y, as is F_{IA}, and it obeys the sum rules [17]

$$\int_{-\infty}^{\infty} dY Y^n \Delta F(Y) = 0, \; n = 0, 1, 2. \tag{6.30}$$

One can show that, for a nodeless ground state, this implies that F is suppressed at $Y = 0$, and it is therefore enhanced on both sides of the quasielastic peak.

6.5 Comparison with Silver's Theory of FSI

It is interesting to compare the "eikonal" theory of final state interactions, developed in the previous section, to the very popular Hohenberg-Platzman ansatz [1] and to the closely related theory by Silver [15]. There, the FSI are described by a convolution function $R(Y)$, defined in Eq. 2.16. With $\hat{}$ denoting Fourier transform with respect to Y, we obtain

$$\hat{F}(s) = \hat{F}_{IA}(s)\hat{R}(s),$$

which can be viewed trivially as the definition of $\hat{R}(s)$. From Eqs. 3.13 and 3.22, we find

$$\hat{F}_{IA}(s) = \int dx \varrho(x, x - s\hat{q}),$$

while transforming Eq. 6.24 yields

$$\hat{F}(s) = \int dx \varrho(x, x - s\hat{q}) \exp\left(is/q \int_0^1 d\sigma (V_{eff}(x - s\hat{q}\sigma) - V_{eff}(x - s\hat{q}))\right).$$

Thus the final state broadening function is given by the Fourier transform of

$$\hat{R}(s) \equiv \frac{\int dx \varrho(x, x - s\hat{q}) e^{is/q \int_0^1 d\sigma (V_{eff}(x - s\hat{q}\sigma) - V_{eff}(x - s\hat{q}))}}{\int dx \varrho(x, x - s\hat{q})}, \tag{6.31}$$

Hence the final state broadening is expressed as a density matrix average of the eikonal distortions of the recoiling particle wave function; i.e., of the forward transmission amplitude.

Let us consider a hard core potential for concreteness. Then, V_{eff} acts to forbid propagation along paths occupied by another particle in the medium: $e^{iV_{eff}}$ is one,

if the struck particle can recoil freely from 0 to s, and it is zero whenever a collision with the medium happens. Then $\hat{R}(s)$ is the probability that a particle suffers no collisions while moving a distance s on a straight path, calculated by averaging over the density matrix weight of each path. Now, ignoring spatial correlations, this probability is simply an exponential with decay rate given by the mean free path; in this way, we recover the Hohenberg-Platzman approximation (see Eqs. 2.16, 2.17)

$$\hat{R}_{HP}(s) = e^{-|s|\pi a^2 N/V}.$$

This approximation was improved by Silver, who accounted for two-particle spatial correlations during the recoil (see Eq. 2.18), and obtained

$$\hat{R}_S(s) = e^{-(N/V)2\pi \int_0^{|s|} dz \int_0^a dbbg(\sqrt{b^2+z^2})}.$$

6.6 Numerical Results for Hard-Core Potentials

This section is devoted to illustrating the concepts we have exposed with a few numerical examples. We should point out immediately that our aim is to study the $q \to \infty$ limit exactly, but give only a qualitative description of the response at finite momenta. Indeed, while at very high momenta the eikonal approximation is appropriate (and it becomes exact asymptotically), at lower q one would have to compute the exact propagator, following the method explained in a previous section.

We consider here the same interaction we used in the calculations of the previous chapter, modified by introducing a hard core of radius a:

$$\begin{aligned} V(r) &= \infty, \ r < a \\ &= 21 \cosh r, \ r > a. \end{aligned} \tag{6.32}$$

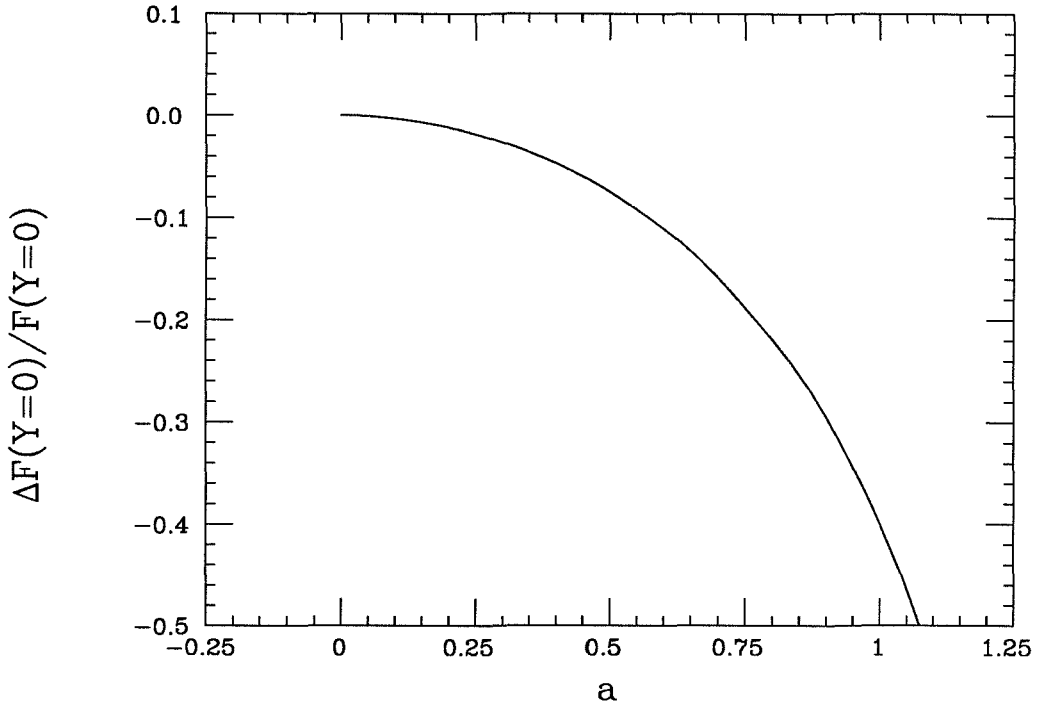

Figure 6.6 – Deviations of the scaling function from the impulse approximation, $\Delta F(0)/F(0)$, for a particle in an attractive potential well, $V(r) = -21\cosh^{-2} r$, with hard core repulsion at $r = a$.

In Fig. 6.6, we plot the deviation from the IA at $Y = 0$, $\Delta F(0)/F(0)$, as a function of the hard core radius (note that we need $a \leq 1.6$ to have a bound state). This curve represents the exact answer, obtained through Eq. 6.29. The scaled response is decreased at $Y = 0$ by the presence of the core. For small a, $\Delta F(0)/F(0) \propto a^2$, as expected from Eq. 6.29, as well as from naive shadowing arguments; as the hard core radius grows, deviations from the IA are stronger than quadratic in a.

Fig. 6.7 shows the results for $F(q, Y = -1.5)$ (compare to Fig. 5.5), obtained by the SPMC method, without treating the hard sphere propagator rigorously, but only imposing the hard core condition that the propagator vanishes inside the core. We have put $a = 0.4$ in this calculation. This obviously reproduces the exact asymptotic

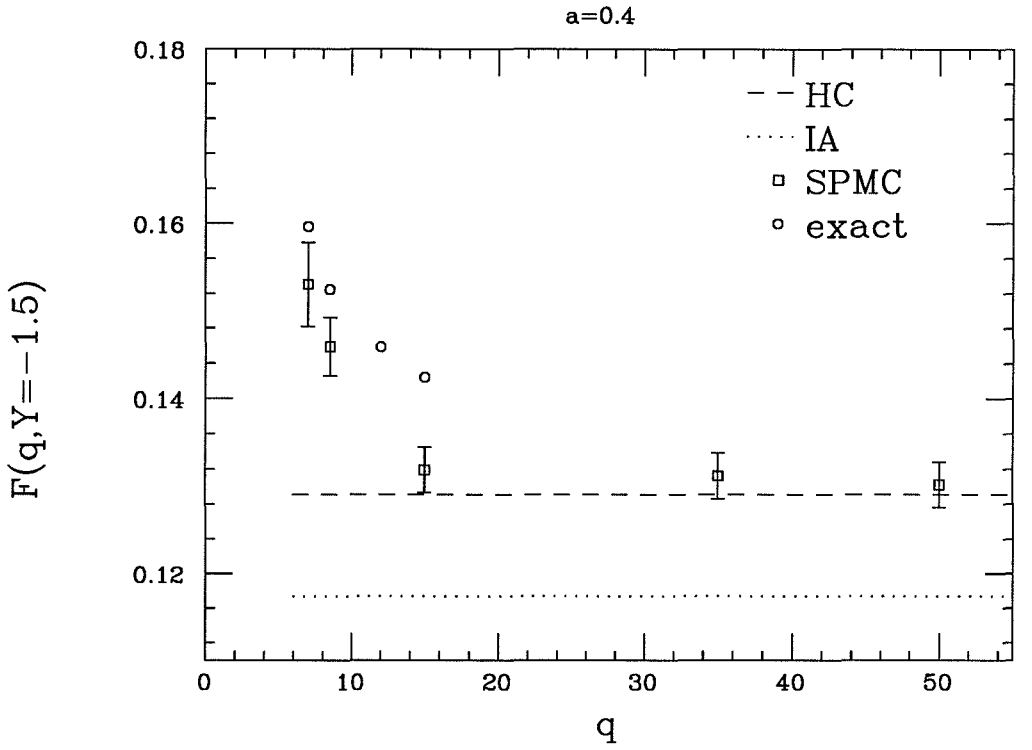

Figure 6.7 – F(q,Y=-1.5) as a function of q. The potential is as in Fig. 6.6, with $a = 0.4$. The circles and the dashed line represent the exact values of F at finite and infinite q respectively. The squares were obtained by the SPMC method. Y-scaling is observed. The scaling function, however, is not the IA (dotted line). Compare to Fig. 5.5, corresponding to the case $a = 0$.

answer, but it appears deficient elsewhere (except at the lower values of q, where the "weak" attractive tail of the potential, which is treated accurately, is most important). Attempts to correct for this by introducing semiclassical representations of the hard-core propagator [38] do not improve the agreement with the (numerically) exact solution. (One should note that, unlike in the case of weak potentials, the exact solution is not easily calculated, nor extrapolated, beyond $q \sim 15$.) The asymptotic limit obtained through the momentum distribution (the IA) is also shown. As expected from the sum rule, this time the IA lies below the true asymptotic value of the response.

Chapter 7
The Response of a ^{4}He Nucleus

7.1 The Experimental Data

The inclusive electron scattering cross section from ^{4}He near the QE peak has been measured at SLAC by the NE3 collaboration, in the experimental range $2.02 \leq E \leq 3.60$ GeV, $15 \leq \theta \leq 30$ degree in the laboratory, and for $Q^2 < 2.8$ GeV^2 [12],[13]. In these references, and in subsequent work [39], the data were analyzed for scaling in the Impulse Approximation (Fig. 7.1), following a method (and a definition of the scaling variable) that is somewhat different from what we have used so far. Because this method is used in virtually all of the nuclear physics literature, we briefly review it, following Ref. [39], and make connection to the formalism we have developed in Chapter 2 (which is based on Ref. [2]).

One starts by assuming that the cross section is given, in the Impulse Approximation, by the single nucleon elastic cross section folded into the nucleon momentum distribution (taken to be the same for the N neutrons and Z protons):

$$\frac{d\sigma}{d\Omega' dE'} = \int \frac{d^3k}{(2\pi)^3} \Big(Z \Big(\frac{d\sigma}{d\Omega'} \Big)_{ep} + N \Big(\frac{d\sigma}{d\Omega'} \Big)_{en} \Big) n(k), \tag{7.1}$$

with the electron-nucleon cross sections given by

$$\frac{d\sigma}{d\Omega'}_{ep(en)} = \sigma'_{ep(en)} \frac{M}{E'} \delta(E - E' + E_f - E_i).$$

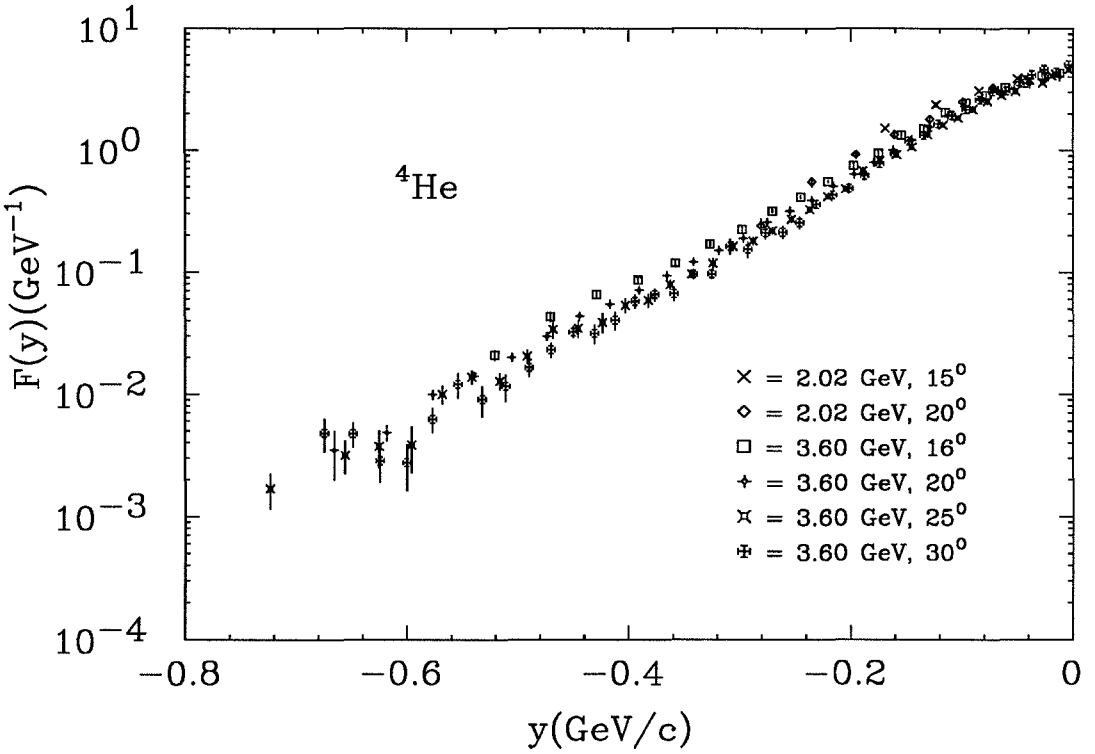

Figure 7.1 – The dynamic response of the ^{4}He nucleus, measured by inclusive electron scattering, on the low energy transfer side of the QE peak (from Ref. [13]). Different curves correspond to different beam energies and scattering angles.

Here $E_{i(f)}$ denote the initial (final)-state energy of the struck nucleon, and σ' is the Mott cross section multiplied by a combination of nucleon form factors, depending only upon the 4-momentum transfer squared $Q^2 \equiv q^2 - \omega^2$. The δ function enforces (relativistic) energy conservation:

$$\omega + M_A = \sqrt{(\vec{q} + \vec{k})^2 + M^2} + \sqrt{M_{A-1}^{*2} + k^2}. \tag{7.2}$$

M_A is the rest mass of the target, M_{A-1}^* is the mass of the recoiling nucleus (possibly in an excited state), and one often defines the quantity ϵ through

$$M_A \equiv M_{A-1}^* + M - \epsilon\,. \tag{7.3}$$

Putting all this into Eq. 7.1, one obtains

$$\frac{d\sigma}{d\Omega' dE'} = (Z\sigma'_{ep} + N\sigma'_{en})\frac{M}{q}\int_{|p_{min}|}^{p_{max}} \frac{dp}{(2\pi)^2} pn(p) \tag{7.4}$$

where, neglecting the kinetic energy of the recoiling nucleus,

$$\begin{aligned} p_{min} &= -q + \sqrt{2M(\omega+\epsilon) + (\omega+\epsilon)^2} \\ p_{max} &= p_{min} + 2q. \end{aligned} \tag{7.5}$$

Now observe that, in the $q \rightarrow \infty$ limit, one can write

$$y_{rel} \equiv p_{min} = -q + \sqrt{2M(\omega+\epsilon) + (\omega+\epsilon)^2} \tag{7.6}$$

and thus

$$\begin{aligned} F(y_{rel}) &= \frac{1}{Z\sigma'_{ep} + N\sigma'_{en}} \frac{q}{M} \frac{d\sigma}{d\Omega' dE'} \\ &= \int_{y_{rel}}^{\infty} \frac{dp}{(2\pi)^2} pn(p). \end{aligned} \tag{7.7}$$

This looks again like y-scaling, but we use lowercase y to stress the difference between the present discussion and our previous derivation of scaling in Chapter 2 and Chapter 3. If one repeats the steps above with non-relativistic kinematics, one arrives at the following scaling variable:

$$y = -q + \sqrt{2M(\omega+\epsilon)}, \tag{7.8}$$

which of course can also be obtained by expanding y_{rel} in powers of ω/M:

$$y_{rel} \simeq y + \frac{(\omega+\epsilon)^{3/2}}{\sqrt{8M}}. \tag{7.9}$$

The non-relativistic variable y is related to Y as follows:

$$Y = y + \frac{y^2}{2q} - \frac{\epsilon}{q}. \tag{7.10}$$

Hence, y and Y are identical in the $q \rightarrow \infty$ limit, as they should be!

7.2 Numerical Computation

In this section, we describe our non-relativistic numerical computation of the quasielastic response of a schematic ^{4}He nucleus; that is, of a collection of four point-like nucleons interacting through the two-body potential specified in Eq. 6.12 (also see Figs. 6.1 and 6.2). We include the Coulomb potential (Eq. 6.13) between the two protons, which amounts to a very small correction to the nuclear interaction.

According to Eq. 3.13, the first step consists in obtaining the ground state density matrix. Because we are dealing with a four-body problem, this alone involves quite a considerable amount of work. For instance, stochastic methods, such as Green's Function Monte Carlo [40] and Path Integral Monte Carlo [10] have been applied to this problem. For our purpose here, it will suffice to use a good "trial" wave function, such as the one employed in the calculations of Ref. [10]. This consists of a totally antisymmetric spin-isospin wave function, multiplied by a spatial totally symmetric Jastrow function

$$\psi(r_1, r_2, r_3, r_4) = \prod_{i<j}^{4} f(r_{ij}) \tag{7.11}$$

with

$$f(r) = e^{-r^2/2r_0^2}\left(1 - \zeta e^{-r/2b}\right)^{\eta}. \tag{7.12}$$

Because the symmetry of the spatial wave function is preserved by time evolution under our hamiltonian, our computation is effectively dealing with a system of four bosons and thus we need not worry about the famed "minus sign problem"

encountered in Monte Carlo simulations of systems of fermions. The parameters of the wave function were optimized in Ref. [10], the optimal choice being

$$\eta = 3.64$$

$$\zeta = 0.46$$

$$r_0 = 2.6 \text{ fm}$$

$$b = 0.15 \text{ fm}.$$

With this choice, the variational ground state energy turns out to be

$$E_0 \simeq 26\text{MeV},$$

rather close to the experimental value of 28.2 MeV, and the QE response in the IA is shown in Fig. 7.2 together with the experimental data (we explain below how the IA was obtained). The good qualitative agreement of the IA calculation shown in Fig. 7.2 assures us of the quality of the trial ground state wave function (7.11).

At this point, one is able to generate the initial and final ground state configurations of the four nucleons, $\{\vec{r}_i\}$, $\{\vec{r}'_i\}$. As before (see Chapter 5), we define the new variables

$$\vec{R}_i = (\vec{r}_i + \vec{r}'_i)/2$$

$$\vec{l}_i = (\vec{r}_i - \vec{r}'_i).$$

From the ground state wave function, we generate $\{\vec{R}_i\}$ and l_z (hereafter, $l_z \equiv (z_1 - z'_1)$ shall refer to the struck particle, and z is chosen in the direction of the momentum transfer, while $\{l_\perp\}$ shall refer to all other transverse coordinate differences). This is done via the Metropolis algorithm [34], by standard Monte Carlo, i.e., by sampling the weight

$$\varrho(\vec{R}_i + l_z/2, \vec{R}_i - l_z/2) \equiv \psi(\vec{R}_1 + \hat{z}l_z/2, \vec{R}_2, \vec{R}_3, \vec{R}_4) \times \psi(\vec{R}_1 - \hat{z}l_z/2, \vec{R}_2, \vec{R}_3, \vec{R}_4).$$

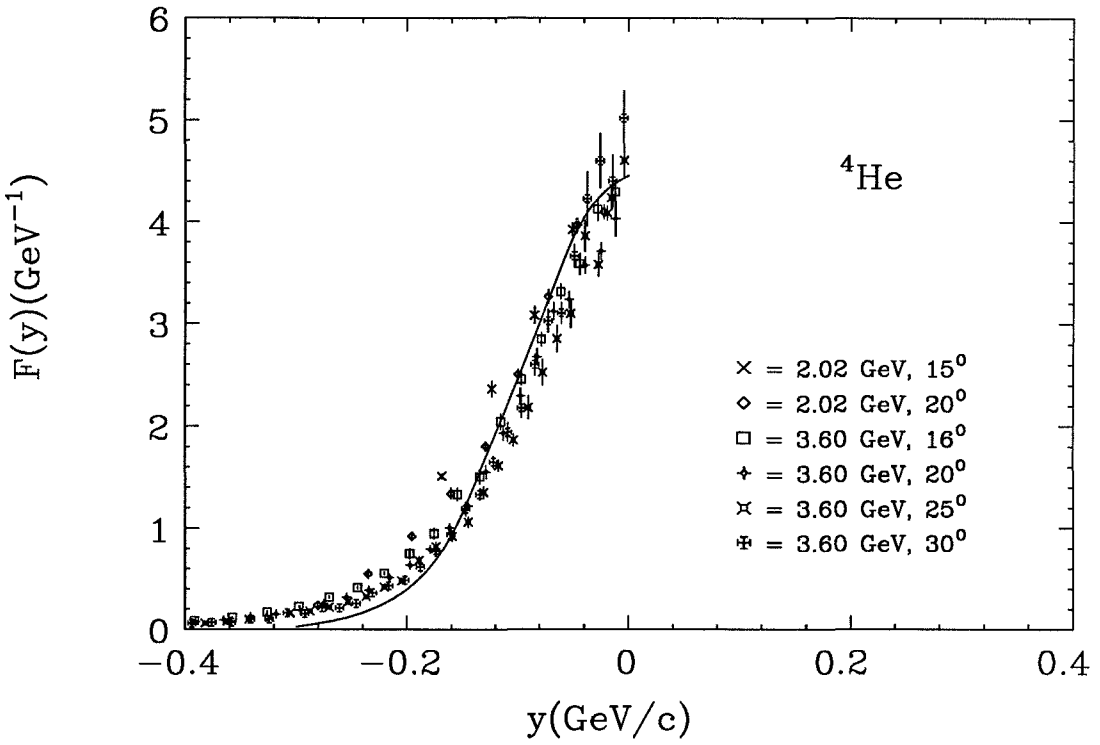

Figure 7.2 – The dynamic response of the 4He nucleus: a comparison between experimental data and the Impulse Approximation assuming a trial ground state wave function (Eqs. 7.11, 7.12). Note the linear scale.

One must be careful to avoid self-correlations between subsequent samplings of the observable (in our case, the response); a simple check is provided by computing the autocorrelation function of a sequence of measurements [20]. As already observed, the normalization of our weight is

$$\int d^3R_1 d^3R_2 d^3R_3 d^3R_4 dl_z \varrho(\vec{R}_i + l_z/2, \vec{R}_i - l_z/2) = 2\pi q S_{IA}(Y=0),$$

so it is known once the IA is calculated. This is done folding Eq. 3.22 into Eq. 3.13. The resulting expression is amenable to Monte Carlo integration, once we write it in the form

$$F_{IA}(Y) = \left\langle \int dl \frac{\psi(\vec{R}_1 - \hat{z}l, \vec{R}_2, \vec{R}_3, \vec{R}_4)}{\psi(\vec{R}_1, \vec{R}_2, \vec{R}_3, \vec{R}_4)} \frac{e^{-iYl}}{2\pi} \right\rangle_{\psi^2}.$$

The one dimensional l integral is carried out by Simpson's rule.

The remaining coordinates describing the ground state configuration, $\{\vec{l}_\perp\}$, are found expanding the potential in Eq. 3.19 linearly in v/q, so that the v integral in Eq. 3.18 becomes

$$\int \frac{d^{11}v}{(2\pi)^{11}} e^{-ivl_\perp} e^{-i(\frac{ml_z}{q})^2(V'_+ - V'_-)v/2m} = \delta^{11}\Big(l_\perp + \frac{1}{2m}(V'_+ - V'_-)(\frac{ml_z}{q})^2\Big)$$

where V' denotes average of the gradient of the potential along the eikonal path of the system. This indicates that the transverse coordinates sample a very small region of the density matrix, proportional to Ft^2, where F is some average force (mean field), plus terms of order t^3 or higher. In this way, we complete our ground state averaging, and can turn to Eq. 3.19.

Because the motion of the center of mass is free and thus the path integral associated with it is trivial, we find it convenient to generate the paths in the center of mass coordinate system: in this way we deal with $9 \times 2N$ rather than $(12 \times 2N)$-dimensional integrals. Because, as was done in Chapter 5, we want to generate the paths using Eq. 4.20 and gaussian random number generation, we need to find a set of coordinates that diagonalize the kinetic energy in the center of mass. One of these is proportional to the "Jacobi coordinates." Choosing the coordinates of particles 2, 3 and 4 $(\vec{\zeta}_2, \vec{\zeta}_3, \vec{\zeta}_4)$ to be independent variables $(\vec{\zeta}_1 = -\vec{\zeta}_2 - \vec{\zeta}_3 - \vec{\zeta}_4)$, the new variables

$$\vec{\alpha} \equiv \frac{2}{\sqrt{3}}(\vec{\zeta}_1 + \vec{\zeta}_2 + \vec{\zeta}_3)$$
$$\vec{\beta} \equiv \frac{1}{\sqrt{6}}(\vec{\zeta}_1 + \vec{\zeta}_2 - 2\vec{\zeta}_3)$$
$$\vec{\gamma} \equiv \frac{1}{\sqrt{2}}(\vec{\zeta}_1 - \vec{\zeta}_2)$$

make the kinetic energy diagonal and do not change the mass. It is easy to see that the new coordinates still vanish at the endpoints, making it possible to define a sine

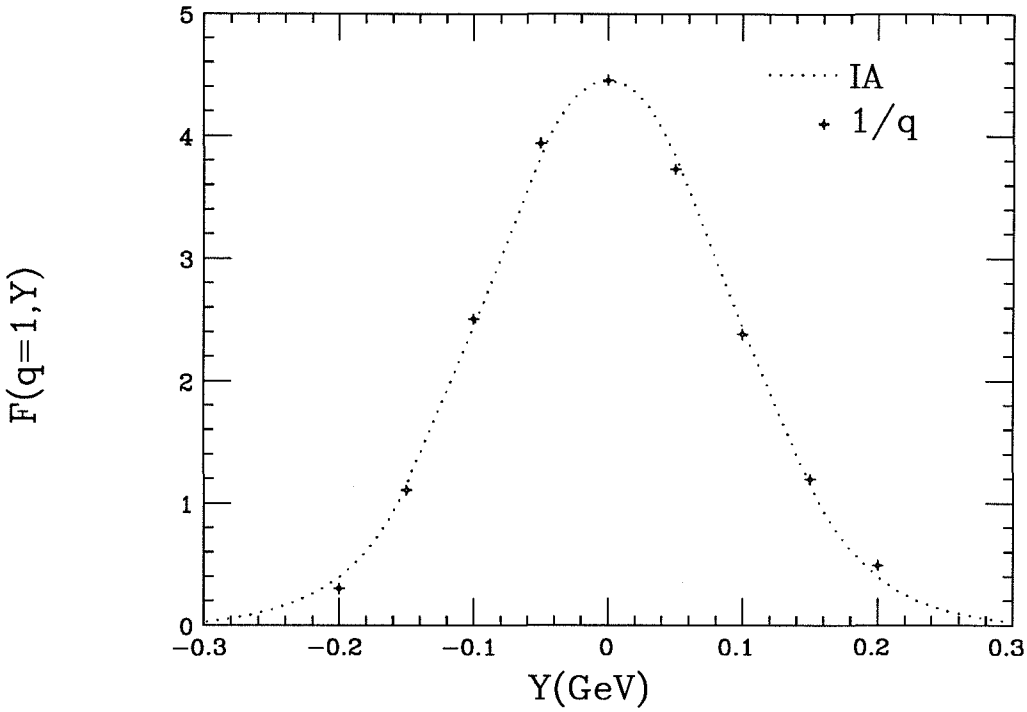

Figure 7.3 – Impulse Approximation and $O(1/q)$ scaling violation for a ^{4}He nucleus described by the wavefunction (7.11) and a state-independent Malfliet-Tjon potential.

transform, as in Eq. 3.20. Once we generate the path, we transform back to the $\{\zeta\}$ coordinates, where the evaluation of the potential is simpler.

The pairwise potential is taken to be the Malfliet-Tjon interaction introduced in Sec. 6.2, and renormalized at short distances through the logarithm of the exact two-body density matrix, as described in Sec. 6.3; the Coulomb interaction also acts between the two protons. Because the effective potential is now non-local, implementing the derivatives in Eq. 4.20 turns out to be an extremely hard and tedious task. Fortunately, the exact density matrix is in general quite small and smooth in the region where we need to use it. This means that the effective potential has a negative (damping) imaginary part and a small derivative. Therefore the derivative

correction in Eq. 4.20 can be safely ignored. However, we account for it when dealing with the "regular" part of the interaction, or when using the full potential directly (at larger separations), though even in these cases, we find that this term has a rather small effect.

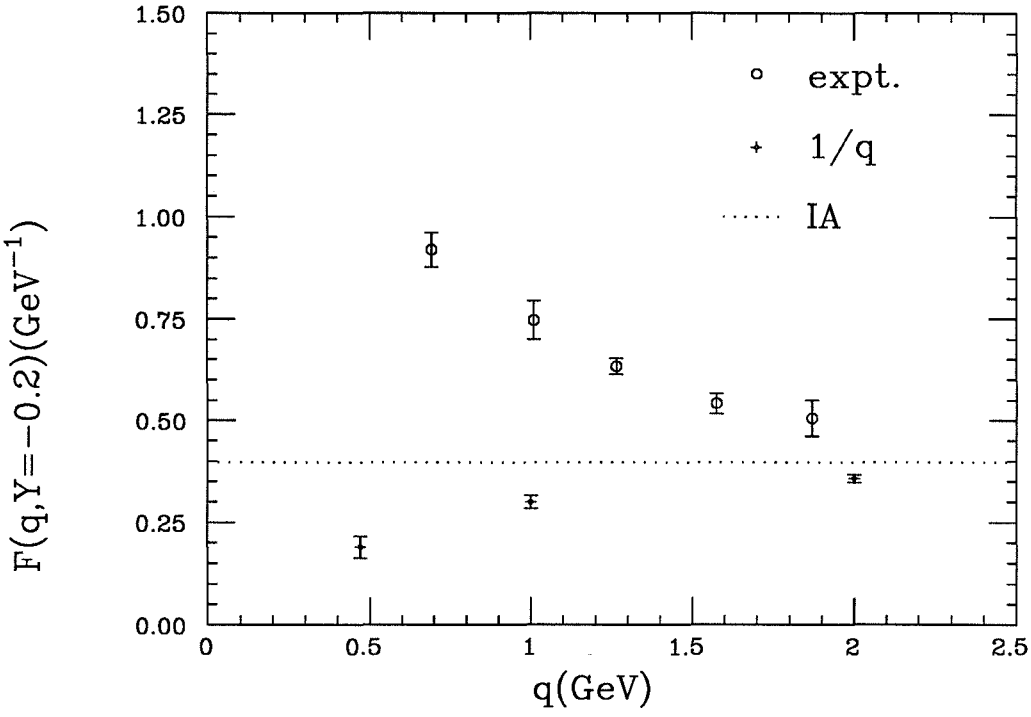

Figure 7.4 – Experimental approach to scaling in ^{4}He ($Y = -0.2$ GeV) compared to the $1/q$ scaling violation.

7.3 Results and Discussion

We start out by investigating the magnitude of the $O(1/q)$ correction to scaling (Eq. 3.24), whose calculation does not require evaluating real time path integrals. Fig. 7.3 shows the scaled response for $|Y| \leq 0.2$ GeV through order $1/q$, for $q = 1$ GeV: the magnitude of the asymmetric correction to the IA is rather small, yet it doesn't seem to reproduce the trend in the experimental data. This is made clearer in

Fig. 7.4, which compares the behavior of the experimental response at fixed $Y = -0.2$ GeV, as a function of q, with the calculated $O(1/q)$ scaling violations. The latter would indicate that $Y-$scaling is approached fairly quickly, as the momentum transfer reaches ~ 1 GeV, from below.

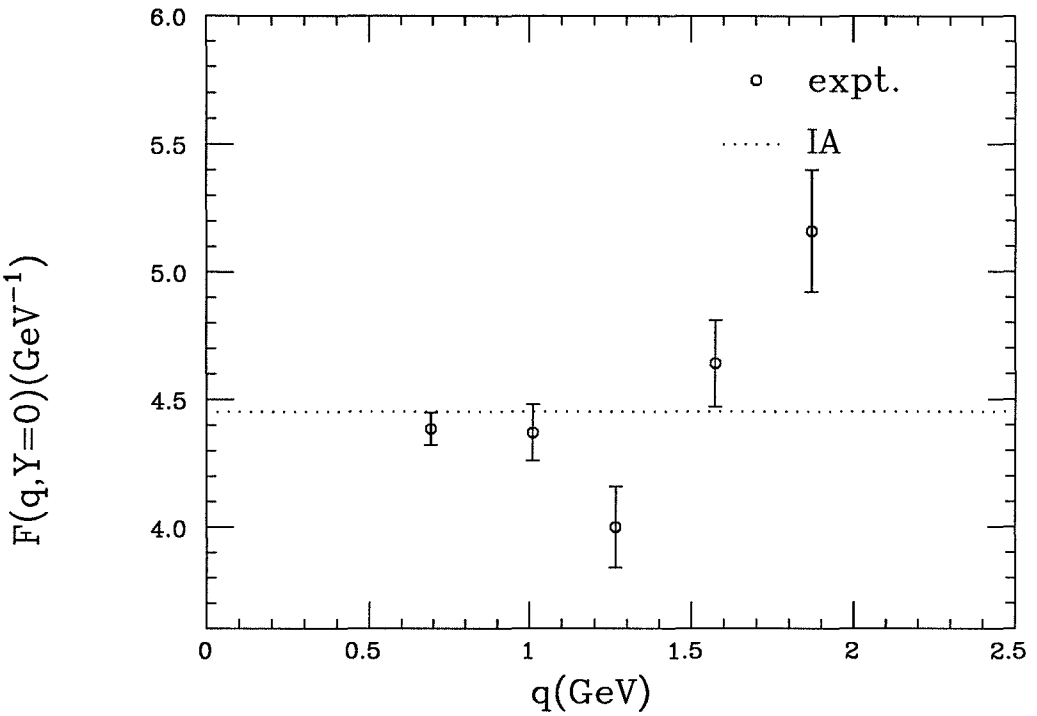

Figure 7.5 – Experimental approach to scaling at $Y = 0$.

The experimental data show opposite behavior. The observed approach to scaling is from below near the top of the quasielastic peak (see Fig. 7.5), whereas the $O(1/q)$ correction vanishes at $Y = 0$ and is positive (but small) for $|Y| < 0.1$ GeV (see Fig. 7.3). On the other hand, for larger $|Y|$, the experimental response is a decreasing function of q, which contrasts with what we saw in Fig. 7.4. This is not very surprising, as we mentioned in previous occasions; it is simply an indication that

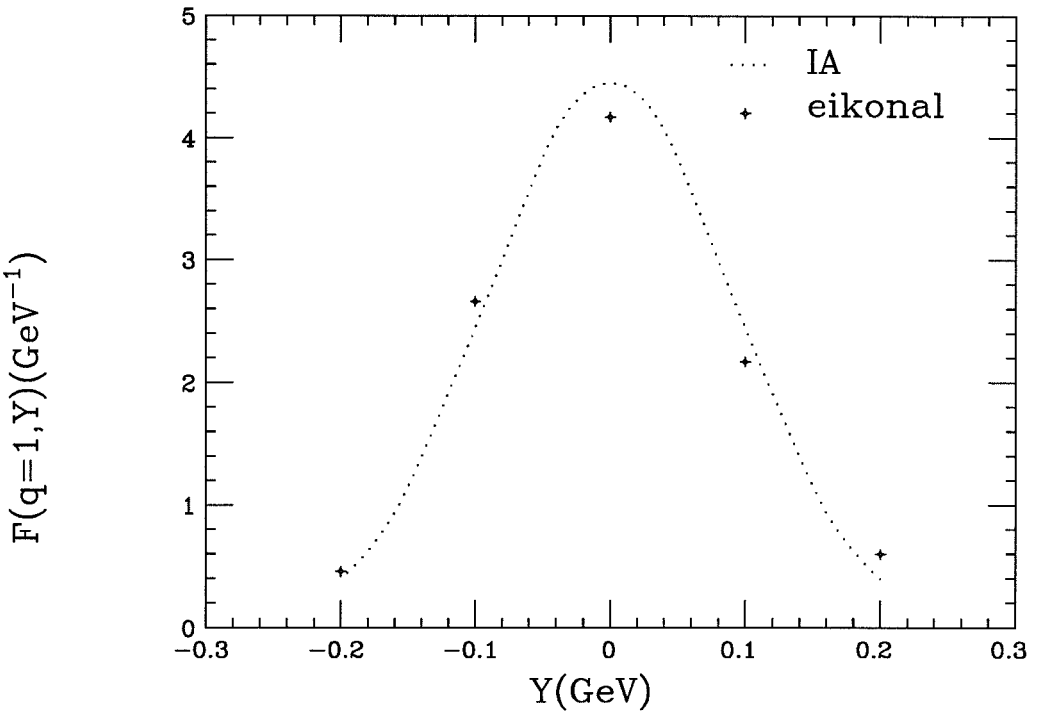

Figure 7.6 – Impulse Approximation and eikonal approximation to the quasielastic response at $q = 1$GeV (compare to Fig. 7.3; here the error bars in the calculation –not shown– are larger).

a V/q expansion is not appropriate for strong potentials. Gersch *et al.*, who first calculated the $1/q$ scaling violations for LHe [9], were well aware of this problem.

Here, we can go a step further, much as we did in Sec. 6.4 for the hard core potential. In fact, we can argue again that the high momentum transfer limit of the response is given by Eq. 6.24, where the effective potential this time is nothing but the logarithm of the exact two-nucleon propagator, derived in Secs. 6.1-6.3. The resulting structure factor contains now all orders in V/q, and should contain the essential physics; in particular, it should describe the approach to scaling correctly. This is indeed what the calculations show; note that these do not involve computing

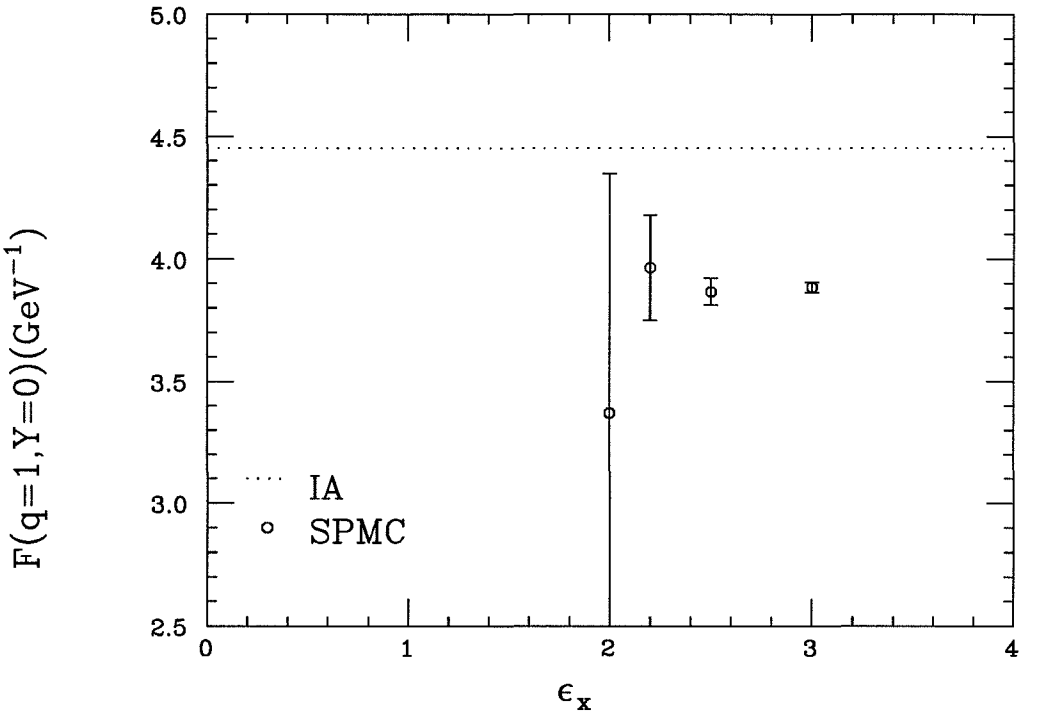

Figure 7.7 – SPMC calculations of $F(q = 1, Y = 0)$ for various values of ϵ_x (see Fig. 5.2).

with path integrals in real time, and bear only a statistical error associated with sampling the ground state wave function stochastically.

Finally, we have performed the real time path integral Monte Carlo calculations. We chose to use the same values of the parameters (ϵ_x, ϵ_l) that we used for our model problem in Chapter 5 (ϵ_x=2.2, ϵ_l=1). The sensitivity of the calculation to ϵ_x is shown in Fig. 7.7. We considered doing an extrapolation to $\epsilon_x = 0$. However, any attempt to improve on the rather obvious (by inspection) fit to a constant is practically meaningless, on a small data sample, because of the fast growing error bars for smaller ϵ_x.

Fig. 7.8 shows the calculated quasielastic response function at $Y = 0$, together with the eikonal approximation and the experimental data. The theoretical scaling

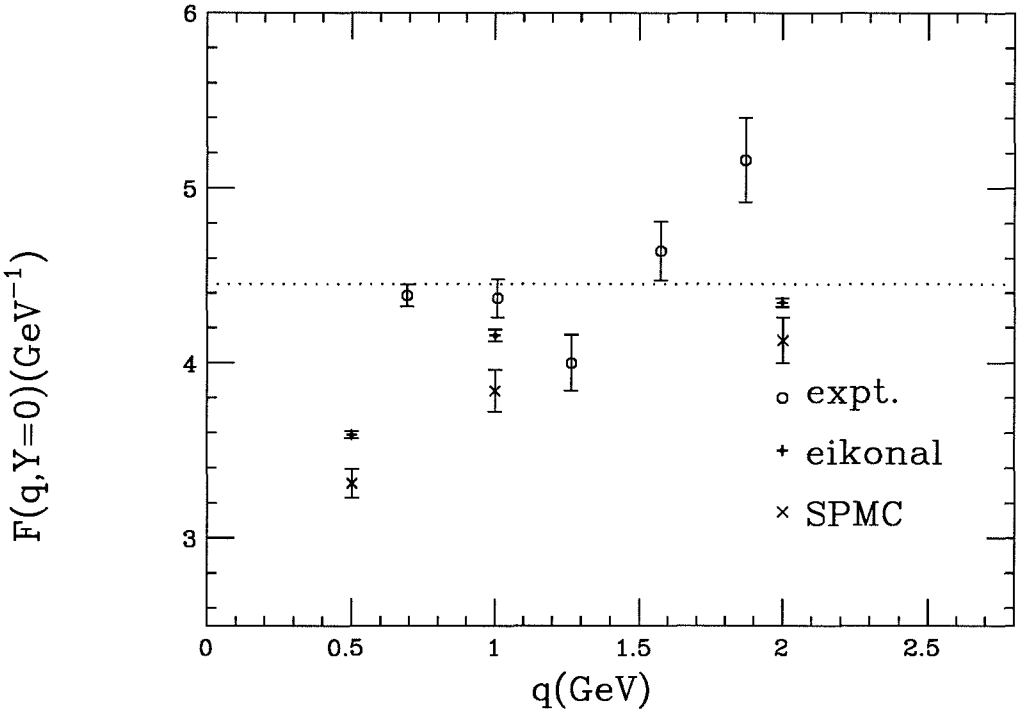

Figure 7.8 – Approach to scaling at $Y = 0$. The dotted line is the theoretical scaling function, the IA (this does not coincide with the experimental scaling function, because of of deficiency of our trial wavefunction, and also because the experimental points are rather sensitive to inelastic "noise" at $Y = 0$.) Note that both SPMC and eikonal approximation (to which the former converges at high q) show a small residual $q-$dependence at the highest experimental q.

does not coincide with the experimental one, presumably because of deficiency of our trial wavefunction, and also because the experimental points are rather sensitive to inelastic "noise" at $Y = 0$. Note that both SPMC and eikonal approximation (to which the former converges at high q) show a small residual $q-$dependence at the highest experimental q. Of course, one should be cautious in making quantitative statements for large q, based on our calculation: relativistic effects are expected to be important at the highest Q^2 reached in the experiment.

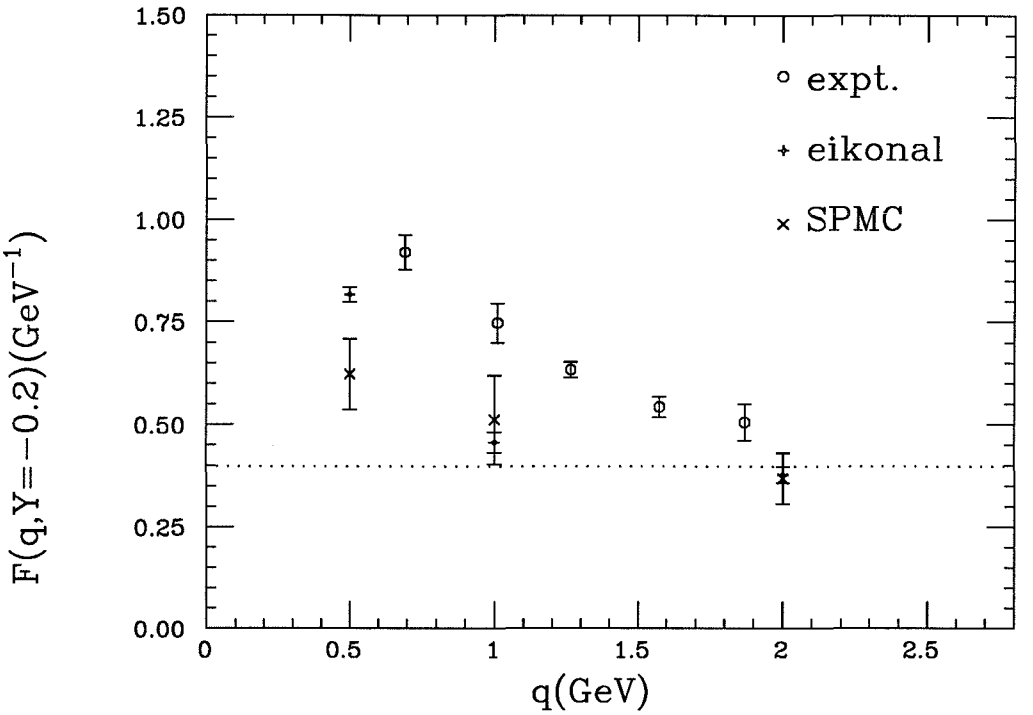

Figure 7.9 – Approach to scaling at $Y = -0.2$ GeV. The dotted line is the theoretical scaling function, the IA.

Fig. 7.9 shows the response at $Y = -0.2$ GeV. Contrary to what we saw in the $Y = 0$ case, here scaling is approached from above. Because the overall behavior of the approach to scaling, as a function of Y, is remarkably different from what expected based on the $1/q$ correction (Eq. 3.24), this means that non-perturbative effects are dominant. This contrasts with what we found in our model problem in Chapter 5; there the potential was lacking the important short range repulsion.

Fig. 7.10 shows the scaling violations at $q = 1$ GeV, normalized to the response function at the highest experimental momentum transfer ($F(q = 1, Y)/F(q = 2, Y) - 1$). This comparison should be quite insensitive to the actual value of the

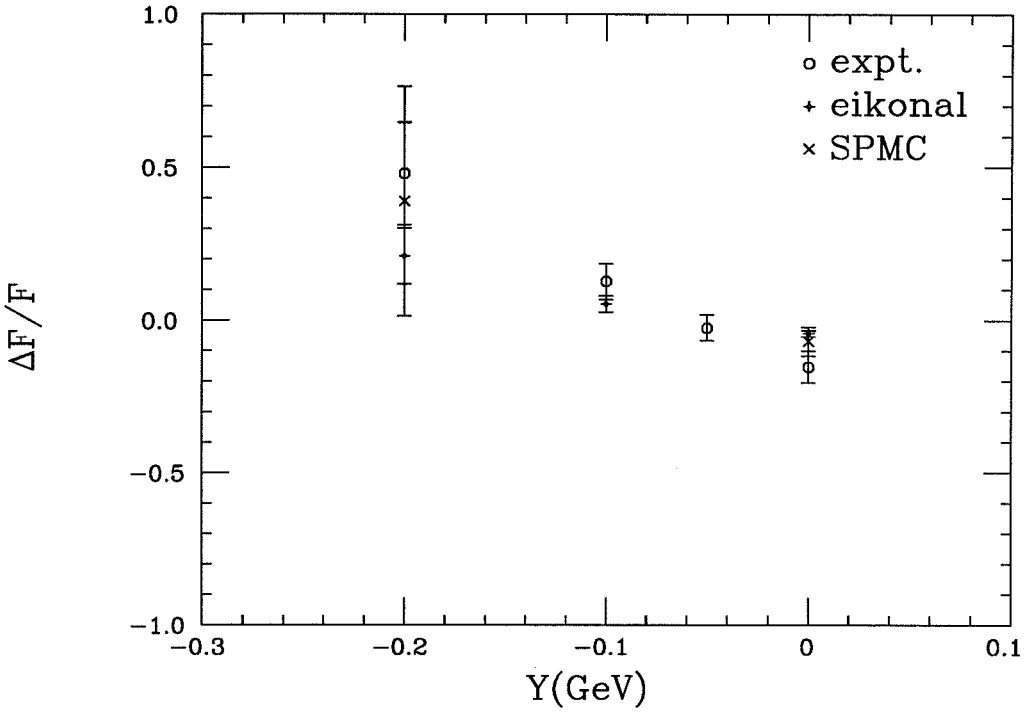

Figure 7.10 – Scaling violations at $q = 1$ GeV, normalized to the response function at the highest momentum transfer achieved in the experiment ($F(q = 1, Y)/F(q = 2, Y) - 1$). This comparison should be quite insensitive to the actual value of the scaling function (i.e., to fine details in the potential and in the trial wavefunction). Note that the sign of the scaling violations has a cross-over at $Y \sim 70$ MeV. This is well reproduced by our calculation, and should be attributed to the short range repulsion in the nuclear force.

scaling function and in general to any systematic source of discrepancy between experiment and theoretical calculations (i.e., to fine details in the potential and in the trial wavefunction).

It is curious to observe that the scaling violations in the ^{4}He nucleus have the same qualitative behavior seen in Sec. 6.5 for the hard core potential; that is, the response lies below the IA around the top of the QE peak, and above it on the sides. Two main differences should be stressed. First, the scaling function, for the

nuclear potential we used, is indeed the IA (this must be the case if the potential is not rigorously hard core). Second, while in the calculations presented in Sec. 6.5, the $q \rightarrow \infty$ limit allowed us to explain the behavior of the scaling function (relative to the IA) invoking the sum rule (the area under the QE peak is fixed), this argument is not rigorous in the present calculation, because the sum rule is valid only in the $q = \infty$ limit. It becomes qualitatively valid, however, in the spirit of Silver's discussion, i.e., if one defines an effective ($q-$dependent) hard core, as explained in Sec. 2.3.

Chapter 8
Summary and Conclusions

This thesis was concerned with quasielastic scattering from quantum many-body systems, and with the possibility of extracting the one-body momentum distribution from the measured dynamic response, in the "Y-scaling" regime. We have emphasized that this problem is common to quite distinct fields in physics. The formalism we have developed, separating the initial state (static) properties from the final state (dynamic) interactions, allows in principle calculations for any system, given the interaction potential.

Driven by the success of stochastic methods in computing equilibrium properties with arbitrary accuracy, we have explored the possibility of developing similar methods for dynamic properties. At present, this looks feasible only for very small systems. In fact, the calculations of Chapter 5 and Chapter 7 are the first of this kind ever performed. Future work should attempt to compare real time Monte Carlo calculations with analytic continuation of imaginary time Monte Carlo data. Because this technique, too, has shown promise only in the last year [7], this issue is completely unexplored so far.

We have been able to understand the approach to scaling in QE scattering from ^{4}He, and explain its behavior as a function of the scaling variable Y. Scaling is approached in the same way expected for a hard core potential; that is, from below near the top of the QE peak, and from above on the sides (of course, unambiguous experimental data are available only on the left side of the peak). However, unlike

in the case of a true hard core, the scaling limit of the QE response was shown to be the IA, thus establishing the connection between the dynamic response and the momentum distribution.

Our calculations of a ^{4}He nucleus, where the nucleons interact via a strongly repulsive potential, have underscored the importance of renormalizing the potential through the exact density matrix. This idea, already employed in static calculations of liquid and solid He, was suggestive of a method for treating truly hard core potentials. We were able to write the exact expression for the scaling function in this case.

Furthermore, the use of the renormalized potential together with an eikonal approximation of the path integral has proven to be able to grasp much of the interesting physics of the ^{4}He nucleus. Extension to larger systems, in particular liquid ^{4}He, appears at this point straightforward (to the extent a path integral Monte Carlo calculation of the density matrix of He clusters at zero temperature can be called such). This would be quite interesting, because for quantum liquids, where the interparticle potential is considerably harder that in nuclei, the experimental scaling function is not expected to be the IA.

Finally, our calculations, being completely non-relativistic, cannot be extended to larger $|Y|$ (in the nuclear physics case) in any simple way. The momentum distribution of atomic nuclei at large $|Y|$ (to measure which, by the way, is the reason the experiments were done), is still to be understood. In West's words [41], "Perhaps one of the most peculiar aspects of the nuclear data is that, over a considerable range of Y, $F(Y) \sim e^{-a|Y|}$. There seems to be no straightforward reason why $F(Y)$ should exhibit such a simple structure."

References

[1] P. C. Hohenberg and P. M. Platzman, Phys. Rev. **152**, 198 (1966).

[2] G. B. West, Phys. Rep. **18**, 263 (1975).

[3] D. M. Ceperley and M. H. Kalos, in *Monte Carlo Methods in Statistical Physics*, K. Binder, ed. (Springer-Verlag, Berlin 1986), pp. 175-189.

[4] E. L. Pollock and D. M. Ceperley, Phys. Rev. **B30**, 2555 (1984).

[5] J. J. Weinstein and J. W. Negele, Phys. Rev. Lett. **49**, 1016 (1982).

[6] P. E. Sokol, Can. J. Phys. **65**, 1393 (1987)

[7] H.-B. Schuettler and D. J. Scalapino, Phys. Rev. Lett. **55**, 1204 (1985); S. R. White, D. J. Scalapino, R. L. Sugar, and N. E. Bickers, Phys. Rev. Lett. **63**, 1523 (1989); M. Jarrel and O. Biham, Phys. Rev. Lett. **63**, 2504 (1989); R. N. Silver, D. S. Sivia, and J. E. Gubernatis, Phys. Rev. **B 41**, 2380 (1990).

[8] J. D. Doll and D. L. Freeman, Adv. Chem. Phys. **73**, 289 (1989); J. D. Doll, D. L. Freeman and M. J. Gillan, Chem. Phys. Lett. **143**, 277 (1988).

[9] H. A. Gersch, L. J. Rodriguez and P. N. Smith, Phys. Rev. **A5**, 1547 (1972).

[10] Y. Alhassid, G. Maddison, K. Langanke, K. Chow, and S. E. Koonin, Z. Phys. **A321**, 677 (1985).

[11] P.E. Sokol, T. R. Sosnick and W. M. Snow, in *Momentum Distributions*, edited by R. Silver and P. Sokol (Plenum, New York, 1989), p. 148.

[12] B. D. Day *et al.*, Phys. Rev. Lett. **59**, 427 (1987).

[13] D. H. Potterveld, Ph.D. Thesis, California Institute of Technology (unpublished).

[14] M. N. Butler and S. E. Koonin, Phys. Lett. **B205**, 123 (1988).

[15] R. N. Silver, Phys. Rev. **B38**, 2283 (1988); Phys. Rev. **B39**, 4022 (1989).

[16] J. W. Clark and R. N. Silver, in *Proceedings of the 1988 Conference on Nuclear Reaction Mechanism*, E. Gadioli, ed. (Ricerca Scientifica ed Educazione Permanente, Milano, 1988), pp.531–540.

[17] S. A. Gurvitz, A. S. Rinat, and R. Rosenfelder, Phys. Rev. C **40**, 1363 (1989).

[18] J. W. Negele and H. Orland, *Quantum Many-particle Systems* (Addison-Wesley, Redwood City, 1988), ch. 2.

[19] A. S. Rinat and R. Rosenfelder, Phys. Lett. **193B**, 411 (1987).

[20] J.W. Negele and H. Orland, *Quantum Many-Particle Systems* (Addison-Wesley, Redwood City, 1988), ch. 8.

[21] J. D. Doll, R. D. Coalson and D. L. Freeman, J. Chem. Phys. **87**, 1641 (1987).

[22] J. D. Doll, T. L. Beck and D. L. Freeman, J. Chem. Phys. **89**, 5753 (1988).

[23] N. Makri and W. H. Miller, Chem. Phys. Lett. **139**, 10 (1987).

[24] J. D. Doll, D. L. Freeman, and T. L. Beck, Adv. Chem. Phys. **77**, in press.

[25] N. Makri and W. H. Miller, J. CHem. Phys. **89**, 2170 (1988).

[26] V. S. Filinov, Nucl. Phys. **B271**, 717 (1986).

[27] S. E. Koonin, in *Nuclear Theory 1981*, edited by G. F. Bertsch (World Scientific, Singapore, 1982), pp. 197-200.

[28] L. Schiff, *Quantum Mechanics* (McGraw-Hill, New York, 1968), ch. 8.

[29] P. M. Morse and H. Feshbach, *Methods of Theoretical Physics* (McGraw-Hill, New York, 1953), p. 719.

[30] P. M. Morse and H. Feshbach, *op. cit.* p. 832.

[31] S. E. Koonin, *Computational Physics* (Benjamin-Cummings, Menlo Park, 1986), ch. 3.

[32] L. D. Landau and E. M. Lifshitz, *Quantum Mechanics*, (Pergamon Press, Oxford, 1977), ch. 3.

[33] M. Abramowitz and I. Stegun, *Handbook of Mathematical Functions* (Dover, New York, 1969).

[34] S. E. Koonin, *Computational Physics* (Benjamin-Cummings, Menlo Park, 1986), ch. 8.

[35] S. M. Callahan, Ph.D. Thesis, California Institute of Technology (1989), unpublished.

[36] R. A. Malfliet and J. A. Tjon, Nucl. Phys. **A127**, 161 (1969).

[37] M. Abramowitz and I. Stegun, *Handbook of Mathematical Functions* (Dover, New York, 1969), ch. 14.

[38] J. A. Barker, J. Chem. Phys. **70**, 2914 (1979).

[39] M. N. Butler and R. D. McKeown, Phys. Lett. B **208**, 171 (1988).

[40] J. G. Zabolitsky and M. H. Kalos, Nucl. Phys. A **356**, 114 (1981).

[41] G. B. West, in *Momentum Distributions*, Silver and Sokol, eds. (Plenum, New York, 1989), p. 109.